New robust nonconforming finite elements of higher order

M. Köster*, A. Ouazzi*, F. Schieweck†, S. Turek*, P. Zajac*

Abstract

We study second order nonconforming finite elements as members of a new family of higher order approaches which behave optimally not only on multilevel refined grids, but also on perturbed grids which are still shape regular but which consist no longer of asymptotically affine equivalent mesh cells. We present two approaches to prevent this order reduction: The first one is based on the use of nonparametric basis functions which are defined as polynomials on the original mesh cell. In the second approach, we define all basis functions on the reference element but add one or more nonconforming cell bubble functions which can be removed at the end by static condensation. For the last approach, we prove optimal estimates for the approximation and consistency error and derive optimal estimates for the discretization error in the case of a Poisson problem. Furthermore, we construct and analyze numerically corresponding geometrical multigrid solvers which are based on the canonical full order grid transfer operators. Based on several benchmark configurations, for scalar Poisson problems as well as for the incompressible Navier-Stokes equations (representing the desired application field of these nonconforming finite elements), we demonstrate the high numerical accuracy, flexibility and efficiency of the discussed new approaches which have been successfully implemented in the FeatFlow software (`www.featflow.de`). The presented results show that the proposed FEM-multigrid combination (together with discontinuous pressure approximations) appear to be very advantageous candidates for realistic flow simulation tools, particularly on (parallel) high performance computing systems.

Keywords: nonconforming FEM, bubble functions, multigrid, error estimates, incompressible Navier-Stokes equations

2000 Mathematics Subject Classification (MSC): 65N15, 65N30, 65N50

*Institut für Angewandte Mathematik, Technische Universität Dortmund, Germany

†Institut für Analysis und Numerik, Otto-von-Guericke-Universität Magdeburg, Postfach 4120, D-39016 Magdeburg, Germany

1 Introduction

Typical grid oriented approaches for solving incompressible CFD problems, for example via finite element, finite volume or finite difference schemes, require the coupling of different physical fields which restricts the choice of the approximation spaces, for instance for pressure and velocity. It turns out that nonconforming finite elements, which impose continuity in a weaker sense only, are perfect candidates to satisfy the corresponding LBB condition, particularly in combination with discontinuous pressure approximations [9, 10, 23]. As an example, Crouzeix and Raviart [24] developed a stable lowest order nonconforming finite element on triangles, resp., tetraeders with piecewise linear velocities and piecewiese constant pressure approximations. In combination with special upwind discretizations [64, 65], also higher Re numbers get feasible in the context of the incompressible Navier-Stokes equations. Moreover, Rannacher and Turek [60] proposed and analyzed a corresponding finite element on quadrilateral, resp., hexehedral meshes which however requires a nonparametric variant to lead to robust and efficient results on arbitary deformed and stretched meshes. Further examples for first order nonconforming finite elements can be found in [34] as well as in [14, 15, 28, 59].

Regarding highly efficient (geometrical) multigrid methods, special solution approaches have been developed in [70, 72] for the stationary as well as nonstationary Navier-Stokes equations, while parallel implementations can be found for 2D in [61, 62] as well as in [11, 12, 57, 58, 66, 73] for the 3D case. Theoretical analysis of multigrid solvers for nonconforming finite elements can be found in [6, 7, 8, 20, 21, 22, 38, 41] as well as in [31] regarding multilevel-splitting approaches. Also for convection-dominated problems, special stabilization techniques for nonconforming finite elements could be derived and analyzed, for instance via FEM upwinding [62, 64, 65], streamline-diffusion [39, 40, 49, 69], interior penalty [13], resp., edge-oriented FEM stabilization [71], high-resolution TVD/FCT techniques [44, 45] and subgrid viscosity methods [2]. In particular, most of these techniques have been realized in the framework of numerical flow simulations based on the Navier-Stokes equations and special extensions, as for instance multiphase flow, turbulence, viscoelastic fluids, heat transfer, so that it can be stated that nowadays nonconforming finite element discretization techniques together with efficient multigrid solvers are well accepted and often used for the numerical simulation of PDEs, particularly for problems arising in structural mechanics and fluid dynamics.

Another important aspect is the accuracy and reliability of numerical approximations which is typically based on a posteriori error estimation. Corresponding techniques have been developed for nonconforming FEM, too, for instance in [1, 16, 17, 18, 19, 26, 27, 32, 36, 42, 63]. Moreover, special techniques for anisotropic grid refinement, for instance in the case of very

small scales of the solution w.r.t. certain directions, could be derived [4, 47, 50, 67, 68] so that nonconforming finite elements of first order have been successfully used for very complex, highly challenging problems in realistic scenarios. Thus, comparing nonconforming finite elements with conforming FEM of the same order, particularly for the solution of incompressible flow problems, the following advantages of nonconforming elements can be stated:

- They allow much more efficient parallel implementations since the degrees of freedom on the element boundary are located at the edges, resp., faces such that the local communication of common data affects at most two elements.

- Due to their special structure, they lead to reduced couplings between pressure and velocity which is advantageous in the framework of discrete projection methods [70] which are preferable for highly nonstationary problems.

- They allow a natural coupling with $H(div)$ elements which is advantageous for porous media [46].

- They allow easier coupling strategies of finite elements w.r.t. different polynomial degree, resp., mesh width since the compatibilty conditions for d-dimensional elements have to be satisfied via $(d-1)$-dimensional faces only.

Up to now, the nonconforming finite elements used in the context of CFD simulations are all of first order only, particularly for complex situations on quite general geometries. However, there exist already theoretical approaches for the construction of corresponding higher order finite elements. Again, Crouzeix and Raviart [24] proposed a nonconforming element of 3rd order. Moreover, Hennart et al. [35] discussed a family of higher order nonconforming finite elements on quadrilateral, resp., hexahedral meshes, while inf-sup-stable element pairs of arbitrary order on triangles can be found by Matthies und Tobiska [56]. Based on the work of Hennart et al. [35], Matthies [52] developed and analyzed families of nonconforming Stokes elements on quadrilaterals for the Stokes equations. Lee and Sheen [48] proposed a new quadratic element on rectangular meshes which is an analogon to the quadratic element of Fortin and Soulie [29] on triangles. Recently, Apel and Matthies [4] analyzed the robustness of nonconforming elements of arbitrary order on anisotropic meshes.

However, all mentioned higher order nonconforming FEM have in common that they have been developed for parallelograms, resp., parallelepipeds only which is not sufficent for realistic applications. Matthies and Schieweck [54] proposed the combination of reference transformations together with modified compatibility conditions between neighboured elements to

reduce the numerical complexity, particularly in 3D. Numerical tests for scalar convection-diffusion problems show the optimal approximation properties on multilevel refined meshes which are based on globally uniform refinements of a given unstructured coarse mesh. These techniques can be extended to hanging node refinements, too, however the case of general shape-regular quadrilateral, resp., hexahedral elements is still open. As an alternative, Rannacher and Turek [60] proposed a special *nonparametric* variant without transformations onto the reference element which however has not been tested yet for higher order finite elements.

Summarizing the state-of-the-art for higher order nonconforming finite elements, we can conclude that, in contrast to the nonconforming first order approaches, they are far from being popular for realistic CFD simulations. On the other hand, numerical studies [25, 30, 37] show the superiority and big potential of higher order approaches, for instance via biquadratic (conforming) velocities and piecewiese linear discontinuous pressure approximations ($\mathbb{Q}_2/\mathbb{P}_1^{dc}$). The corresponding results for the first second order members of a new class of higher order nonconforming finite elements will be presented in this paper which is organized as follows: After introducing the notations and definitions in Section 2, we explain in Section 3 the new class of nonconforming finite elements, while Section 4 and 5 discuss the techniques to get robustness for general meshes. Finally, Section 6 presents the corresponding multigrid solvers which are followed by several numerical test calculations for the incompressible Navier-Stokes equations in Section 7.

2 Notation and Preliminaries

2.1 General Notations

Let $\Omega \subset \mathbb{R}^d$, $d = 2, 3$, be a bounded domain with a polygonal or polyhedral boundary. For a domain $G \subset \Omega$, let $|\cdot|_{m,p,G}$ and $\|\cdot\|_{m,p,G}$ denote the usual seminorm and norm in the Sobolev spaces $W^{m,p}(G)$ and $(W^{m,p}(G))^d$, respectively. For the Hilbert spaces $H^m(G)$ and $(H^m(G))^d$, we omit the index p and denote the seminorm and norm by $|\cdot|_{m,G}$ and $\|\cdot\|_{m,G}$. The inner product in $L^2(G)$ and $(L^2(G))^d$ will be denoted by $(\cdot,\cdot)_G$, whereas for a sufficiently smooth $(d-1)$-dimensional face E of G, the inner product in $L^2(E)$ is denoted by $\langle\cdot,\cdot\rangle_E$. By $\mathbb{P}_m(D)$ we denote the space of all polynomials on the domain $D \subset \mathbb{R}^n$, $1 \le n \le d$, with total degree less than or equal to m and by $\mathbb{Q}_m(D)$ the space of those polynomials where the maximum power in each coordinate is less than or equal to m. For $p \in [1, \infty]$, both the usual p-norm of a vector in $\mathbb{R}^d$ and the induced p-norm of a $d \times d$-matrix are denoted by $\|\cdot\|_p$. For a set $G \subset \mathbb{R}^d$, we denote by $\mathrm{int}(G)$ and $\overline{G}$ the interior and closure of G, respectively. If G is a domain in $\mathbb{R}^d$ we denote by $|G|$ the d-measure of G and if E is a $(d-1)$-dimensional manifold we denote by $|E|$ the $(d-1)$-measure of E.

Let n with $1 \le n \le d$ denote a given dimension, $\mathbb{N}_0$ the set of the non-negative integers, $s \in \mathbb{N}_0$ and $\mathcal{A}_s^{(n)}$ the following set of multi-indices

$$\mathcal{A}_s^{(n)} := \Big\{ \alpha = (\alpha_1, \ldots, \alpha_n) \in \mathbb{N}_0^n : \sum\nolimits_{k=1}^{n} \alpha_k \le s \Big\}.$$

For $i \in \mathbb{N}_0$, let $L_i(t)$ denote the i-th one-dimensional Legendre polynomial normalized such that $L_i(1) = 1$. Then, we define for $\alpha \in \mathcal{A}_s^{(n)}$ the n-dimensional Legendre polynomials with degree of at most s as

$$L_\alpha^{(n)}(\xi) := \prod_{k=1}^{n} L_{\alpha_k}(\xi_k) \qquad \forall\, \xi = (\xi_1, \ldots, \xi_n) \in \mathbb{R}^n,$$

i.e., in particular, we have $L_\alpha^{(1)}(t) = L_\alpha(t)$ for $\alpha \in \mathbb{N}_0$, $t \in \mathbb{R}$. Furthermore, for multi-indices $\alpha, \beta \in \mathbb{N}_0^n$ we denote by $\delta_{\alpha,\beta}$ the Kronecker Delta which is 1 if $\alpha = \beta$ and 0 in all other cases. Throughout this paper, C will denote a generic constant which may have different values at different places. All these constants occurring inside of any estimate will be independent of the local and global mesh parameters h_K and h defined below.

2.2 Multilevel Grids

Let the bounded domain $\Omega \subset \mathbb{R}^d$ be partitioned by a *grid* $\mathcal{T}_h$ consisting of elements $K \in \mathcal{T}_h$ which are assumed to be open quadrilaterals or hexahedra such that $\Omega = \mathrm{int}\big(\bigcup_{K\in\mathcal{T}_h} \overline{K}\big)$. For an element $K \in \mathcal{T}_h$, we denote by h_K the diameter of the element K. The *mesh size* h of $\mathcal{T}_h$ is given by $h := \max_{K\in\mathcal{T}_h} h_K$. We denote by $F_K : \widehat{K} \to K$ the mapping between the reference element $\widehat{K} := (-1,+1)^d$ and the original element K. In the sequel of this paper, the mapping F_K is assumed to be multi-linear, i.e. $F_K \in (\mathbb{Q}_1(\widehat{K}))^d$. Therefore, the two-dimensional faces of 3D hexahedral elements $K \in \mathcal{T}_h$ can be curved in general. The mesh family $\{\mathcal{T}_h\}$ is assumed to be *shape-regular* in the sense presented in [55], see also [53].

We say that $\{\mathcal{T}_h\}$ is a family of *multilevel grids* if it is generated by a refinement process in the following way. We start with an initial partition $\mathcal{T}^0$ of the domain Ω into elements $K \in \mathcal{T}^0$ of grid level 0, i.e. $\Omega = \mathrm{int}\big(\bigcup_{K\in\mathcal{T}^0} \overline{K}\big)$. The grid $\mathcal{T}^0$ is assumed to be *regular* in the usual sense, i.e., the intersection $\overline{K_1} \cap \overline{K_2}$ of any two different elements $K_1, K_2 \in \mathcal{T}^0$ is either empty or a common $(d-m)$-dimensional face of K_1 and K_2 where $m \in \{1, \ldots, d\}$. In order to generate the elements of grid level 1, each element $K \in \mathcal{T}^0$ is refined, i.e., it is split into 2^d new elements of the grid $\mathcal{T}^1$ called *son-elements* of K which are denoted by $\sigma_i(K)$, $i = 1, \ldots, 2^d$, see Figure 1, right. These son-elements are defined as follows: Let $\widehat{K}_i$, $i \in \{1, \ldots, 2^d\}$, be the son-elements of the reference element $\widehat{K} = (-1,1)^d$ which are congruent d-cubes with $|\widehat{K}_i| = 1$, see Figure 1, left. The i-th son-element $\sigma_i(K)$ of the original element K is defined as $\sigma_i(K) := F_K(\widehat{K}_i)$, $i = 1, \ldots, 2^d$. Note that it can happen in the three-dimensional case

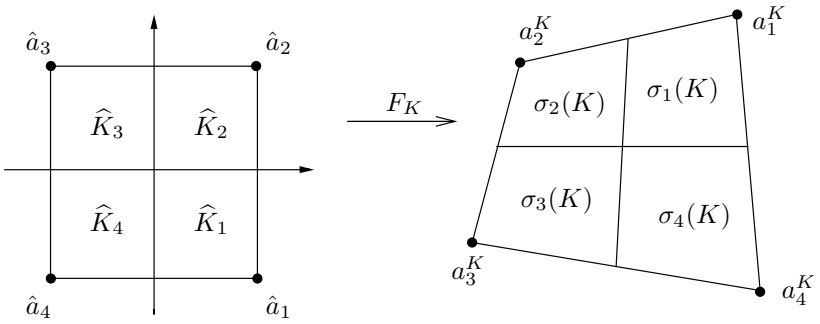

Figure 1: *Refinement of element K into son-elements $\sigma_i(K)$, $i = 1, \ldots, 2^d$.*

that son-elements $\sigma_i(K)$ have curved faces even if the element K has only planar faces, see Remark 3.3 in [51] for an example. Having created the elements of the grid $\mathcal{T}^1$, we continue this refinement process to generate further grids $\mathcal{T}^2, \ \ldots \ , \mathcal{T}^\ell$. Then, our actual grid $\mathcal{T}_h$ is the grid $\mathcal{T}^\ell$ on the finest grid level ℓ. An advantage of multilevel grids is that the reference mapping F_K behaves – up to a power of the mesh size h – like an affine mapping which leads to the following result.

Lemma 1. *Let $\{\mathcal{T}_h\}$ be a family of shape-regular multilevel grids generated from a coarse grid $\mathcal{T}^0$ as described above. Then, there exist constants $C_1(m, \mathcal{T}^0)$, $0 \le m \le d$, such that the estimates*

$$\begin{aligned} |F_K|_{m,\infty,\widehat{K}} &\le C_1(m, \mathcal{T}^0)\, h_K^m \qquad && \forall\, 0 \le m \le d, \\ |F_K|_{m,\infty,\widehat{K}} &= 0 && \forall\, m \ge d+1, \end{aligned} \tag{1}$$

are satisfied for all $K \in \mathcal{T}_h$.

Proof. See Lemma 5 in [53]. □

These properties for the reference mapping in the case of multilevel grids are essential to prove that the so-called *parametric version* of the nonconforming elements, where the basis is defined on the reference element, has optimal aproximation properties [53].

Finally, we introduce some notation to describe the element faces. For an element $K \in \mathcal{T}_h$, we denote by $\mathcal{E}(K)$ the set of all $(d-1)$-dimensional faces of K. Let $\mathcal{E}_h := \bigcup_{K \in \mathcal{T}_h} \mathcal{E}(K)$ be the set of all element faces of the grid $\mathcal{T}_h$. We split $\mathcal{E}_h$ as $\mathcal{E}_h = \mathcal{E}_h^i \cup \mathcal{E}_h^b$ where $\mathcal{E}_h^i$ denotes the set of all inner faces and $\mathcal{E}_h^b$ the set of all faces located at the boundary of Ω. For each inner face $E \in \mathcal{E}_h^i$, there exist exactly two different elements denoted by $K(E)$ and $K'(E)$ such that E is one of their faces. For the boundary faces $E \in \mathcal{E}_h^b$, there is only one element denoted by $K(E)$ which has E as one of its faces and we set formally $K'(E) := \emptyset$. For an element $K \in \mathcal{T}_h$ and a face $E \in \mathcal{E}(K)$, we denote by n_E^K the unit normal on E pointing outward with respect to K. We assign to each face $E \in \mathcal{E}_h$ the unit normal $n_E := n_E^{K(E)}$.

3 Parametric version of nonconforming higher order elements

3.1 Parametric nonconforming FE spaces

In the following, we present the approach of [54] for a parametric definition of a nonconforming FE space via the fixed reference element combined with a new compatibility condition. Let $r \geq 1$ denote the fixed degree of our finite element space and let us suppose that we have already defined the finite element $\big(\widehat{K}, \widehat{V}_r, \widehat{\mathcal{N}}_r\big)$ on the reference cell $\widehat{K} = (-1,1)^d$ with the function space $\widehat{V}_r$ and the set $\widehat{\mathcal{N}}_r$ of nodal functionals. Then, we define the function space $V_r(K)$ on the original element $K \in \mathcal{T}_h$ as

$$V_r(K) := \big\{ v = \hat{v} \circ F_K^{-1} \ : \ \hat{v} \in \widehat{V}_r \big\}. \tag{2}$$

Let $H^{1,h}(\Omega)$ denote the space of elementwise H^1-functions with respect to $\mathcal{T}_h$, i.e.,

$$H^{1,h}(\Omega) := \{ v \in L^2(\Omega) \ : \ v|_K \in H^1(K) \, \forall K \in \mathcal{T}_h \}. \tag{3}$$

Furthermore, we will introduce the *jump* $[v]_E$ of a function v across a $(d-1)$-dimensional face $E \in \mathcal{E}_h^i$ as

$$[v]_E := \big(v|_{K(E)}\big)\big|_E - \big(v|_{K'(E)}\big)\big|_E \qquad \forall v \in H^{1,h}(\Omega). \tag{4}$$

In the two-dimensional case and in the case of tetrahedral elements, the global nonconforming finite element space is defined by

$$\widetilde{V}_{g,h} := \Bigg\{ v_h \in H^{1,h}(\Omega) : v_h|_K \in V_r(K) \, \forall K \in \mathcal{T}_h, \ \int_E q \, [v_h]_E \, d\gamma = 0 \ \ \forall E \in \mathcal{E}_h^i \ \forall q \in \mathbb{P}_{r-1}(E), \\ \int_E q(v_h - g) \, d\gamma = 0 \ \ \forall E \in \mathcal{E}_h^b \ \forall q \in \mathbb{P}_{r-1}(E) \Bigg\}, \tag{5}$$

see Hypothesis H.2 in [24]. However, if we use this definition also in the case of hexahedral elements we get the following problem: It is not clear what the polynomial space $\mathbb{P}_{r-1}(E)$ means in the general case where the element faces $E \in \mathcal{E}_h$ are curved. Moreover, in this case, the finite element basis functions have to be computed separately for each element by evaluating surface integrals and solving a local linear system of equations which leads to higher computing costs and memory requirements to store these solutions.

Due to these drawbacks, we introduce the global finite element space in a different way. As new compatibility conditions we take

$$\int_{U_{d-1}} q(\xi) \, \big[v_h\big(T_E(\xi)\big) \big]_E \, d\xi = 0 \qquad \forall q \in \mathbb{P}_k(U_{d-1}), \ \ E \in \mathcal{E}_h^i, \tag{6}$$

where $k = r-1$ and $U_m := (-1,1)^m$ is the m-dimensional unit cube. The mapping $T_E : U_{d-1} \to E$ is defined to be the multi-linear transformation

$$T_E(\xi) := F_{K(E)}\big(\widehat{T}_{\widehat{E}}(\xi)\big) \qquad \forall \xi \in U_{d-1} \tag{7}$$

based on an affine mapping $\widehat{T}_{\widehat{E}} : U_{d-1} \to \widehat{E} := F_{K(E)}^{-1}(E)$ which will be defined below. Now, we define our global nonconforming finite element space V_h as

$$V_h := \Big\{ v_h \in H^{1,h}(\Omega) : v_h|_K \in V_r(K) \; \forall K \in \mathcal{T}_h, \;\; v_h \text{ satisfies (6) with } k = r-1 \Big\}. \tag{8}$$

The advantage of the new compatibility condition (6) compared to the usual one in (5) is that in the 3D case only integrals over the unit square U_2 have to be evaluated instead of surface integrals over curved element faces.

For a discrete function $v_h \in V_h$, the continuous Dirichlet boundary condition $u = g$ on $\partial\Omega$ is discretized by

$$\int_{U_{d-1}} q(\xi) \Big\{ v_h\big(T_E(\xi)\big) - g\big(T_E(\xi)\big) \Big\} \, d\xi = 0 \qquad \forall q \in \mathbb{P}_k(U_{d-1}), \;\; E \in \mathcal{E}_h^b, \tag{9}$$

with $k = r-1$. We define the space $V_{g,h}$ to approximate the solution u as

$$V_{g,h} := \Big\{ v_h \in V_h : v_h \text{ satisfies (9) with } k = r-1 \Big\}. \tag{10}$$

Furthermore, let $V_{0,h}$ denote the space $V_{g,h}$ with $g = 0$.

It is easy to show that the space $\widetilde{V}_{g,h}$ in (5) with the usual compatibility condition is identical with our new space $V_{g,h}$ for all grids in the two-dimensional case and for grids $\mathcal{T}_h$ consisting of affine equivalent elements (parallelepipeds) in the three-dimensional case. This is mainly caused by the fact that in these cases the mapping T_E is affine.

3.2 Construction on the reference element

Let $\widehat{\mathcal{E}}$ denote the set of all $(d-1)$-faces of the reference element $\widehat{K} = (-1,1)^d$. In the following, we will define the set $\widehat{\mathcal{N}}_r$ of nodal functionals on the reference element which consists of two subsets. In the first subset, we assign to each face $\widehat{E} \in \widehat{\mathcal{E}}$ and each multi-index $\alpha \in \mathcal{A}_{r-1}^{(d-1)}$ the functional

$$\widehat{N}_{\widehat{E},\alpha}(\widehat{v}) := |\widehat{E}|^{-1} \int_{U_{d-1}} \big(\widehat{v} \circ \widehat{T}_{\widehat{E}}\big)(\xi) L_\alpha^{(d-1)}(\xi) \, d\xi \,, \tag{11}$$

where $\widehat{T}_{\widehat{E}} : U_{d-1} \to \widehat{E}$ is an affine mapping defined as follows, see Figure 2. Let $\widehat{a}_{\widehat{E},i}$, $i = 1, \ldots, 2^{d-1}$, denote the vertices of the face $\widehat{E}$ and $b_{\widehat{E}} := 2^{1-d} \sum_{i=1}^{2^{d-1}} \widehat{a}_{\widehat{E},i}$ the barycenter of $\widehat{E}$. We assume that the vertices are numbered for $d = 2$ from right to left and for $d = 3$ in a counterclockwise sense if one looks from inside of $\widehat{K}$ at $\widehat{E}$. Then, we define

$$\widehat{T}_{\widehat{E}}(\xi) := b_{\widehat{E}} + \sum_{k=1}^{d-1} \xi_k \widehat{r}_{\widehat{E}}^{(k)} \qquad \forall \, \xi = (\xi_1, \ldots, \xi_{d-1}) \in U_{d-1}, \tag{12}$$

where $\widehat{r}_{\widehat{E}}^{(1)} := \frac{1}{2}\big(\widehat{a}_{\widehat{E},2} - \widehat{a}_{\widehat{E},1}\big)$ and, in the case $d = 3$, $\widehat{r}_{\widehat{E}}^{(2)} := \frac{1}{2}\big(\widehat{a}_{\widehat{E},4} - \widehat{a}_{\widehat{E},1}\big)$. In the second subset of nodal functionals, we assign to each multi-index $\beta \in \mathcal{A}_{r-2}^{(d)}$ the functional

$$\widehat{N}_{\widehat{K},\beta}(\widehat{v}) := |\widehat{K}|^{-1} \int_{\widehat{K}} \widehat{v}(\hat{x}) L_\beta^{(d)}(\hat{x}) \, d\hat{x} \,. \tag{13}$$

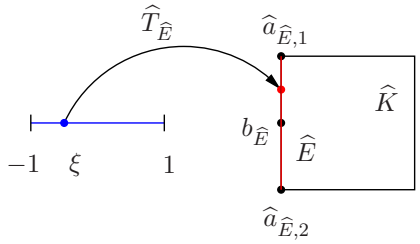

Figure 2: *Mapping* $\widehat{T}_{\widehat{E}} : U_{d-1} \to \widehat{E}$ *for* $d = 2$.

Now, the set $\widehat{\mathcal{N}}_r$ is given by

$$\widehat{\mathcal{N}}_r := \{\widehat{N}_{\widehat{E},\alpha} : \widehat{E} \in \widehat{\mathcal{E}}, \alpha \in \mathcal{A}_{r-1}^{(d-1)}\} \cup \{\widehat{N}_{\widehat{K},\beta} : \beta \in \mathcal{A}_{r-2}^{(d)}\}. \tag{14}$$

After choosing the set $\widehat{\mathcal{N}}_r$ of nodal functionals, we have to look for suitable function spaces $\widehat{V}_r$. A first requirement is that its dimension is equal to the number of nodal functionals in $\widehat{\mathcal{N}}_r$. A second demand is that the polynomial space $\mathbb{P}_r$ should be a subspace of $\widehat{V}_r$ since we want to have finite elements of order r. Moreover, the set $\widehat{\mathcal{N}}_r$ has to be unisolvent on $\widehat{V}_r$.

In [52], three possible families were considered in the two-dimensional case. One of them turned out to be suitable also on anisotropic meshes [3]. Following Hennart et al. [35], we can use for $r = 2$ in the two-dimensional case the local polynomial space

$$\widehat{V}_2 := \mathbb{P}_2(\widehat{K}) \oplus \operatorname{span}\{\hat{x}^2\hat{y}, \hat{x}\hat{y}^2, \hat{x}^3\hat{y} - \hat{x}\hat{y}^3\} \tag{15}$$

and in the three-dimensional case (see Example 10 in [35])

$$\widehat{V}_2 := \mathbb{P}_2(\widehat{K}) \oplus \operatorname{span}\{\hat{x}^2\hat{y}, \hat{x}\hat{y}^2,\ \ \hat{y}^2\hat{z}, \hat{y}\hat{z}^2,\ \ \hat{z}^2\hat{x}, \hat{z}\hat{x}^2,\ \ \hat{x}^3\hat{y} - \hat{x}\hat{y}^3, \hat{y}^3\hat{z} - \hat{y}\hat{z}^3, \hat{z}^3\hat{x} - \hat{z}\hat{x}^3\}. \tag{16}$$

For the case $r = 1$, we use the well-known parametric mean value oriented element of Rannacher and Turek [60].

Due to the unisolvence of $\widehat{\mathcal{N}}_r$ with respect to the space $\widehat{V}_r$, there exists a unique dual basis of $\widehat{V}_r$, i.e.

$$\widehat{V}_r = \operatorname{span}\Big\{\widehat{\phi}_{G,\alpha} : (G,\alpha) \in \Big(\widehat{\mathcal{E}} \times \mathcal{A}_{r-1}^{(d-1)}\Big) \cup \Big(\{\widehat{K}\} \times \mathcal{A}_{r-2}^{(d)}\Big)\Big\} \tag{17}$$

with

$$\widehat{N}_{G,\alpha}\big(\widehat{\phi}_{H,\beta}\big) = \begin{cases} 1, & \text{if } (G,\alpha) = (H,\beta), \\ 0, & \text{otherwise.} \end{cases} \tag{18}$$

The corresponding basis functions can be computed and implemented automatically by means of a computer algebra software package like, for instance, MAPLE. In the following, the basis functions $\widehat{\phi}_{G,\alpha}$ with $(G,\alpha) \in \{\widehat{K}\} \times \mathcal{A}_{r-2}^{(d)}$ are called *nonconforming element-bubble functions* since they are zero on the element boundary in a weaker integral sense.

Finally, we will define the finite element interpolation operator on the reference element $\widehat{\Pi} : H^1(\widehat{K}) \to \widehat{V}_r$. Let us denote by $\{\widehat{N}_{G,\alpha}\}$ the set of all nodal functionals $\widehat{\mathcal{N}}_r$ collecting the face nodal functionals $\widehat{N}_{\widehat{E},\alpha}$ from (11) and the bubble nodal functionals $\widehat{N}_{\widehat{K},\beta}$ from (13). Then, for a given function $\widehat{v} \in H^1(\widehat{K})$, we define the interpolate $\widehat{\Pi}\widehat{v} \in \widehat{V}_r$ by

$$\widehat{\Pi}\,\widehat{v}(\hat{x}) := \sum_{G,\alpha} \widehat{N}_{G,\alpha}(\widehat{v})\phi_{G,\alpha}(\hat{x}). \tag{19}$$

Obviously, the operator $\widehat{\Pi} : H^1(\widehat{K}) \to \widehat{V}_r$ is continuous and satisfies

$$\widehat{\Pi}\,\widehat{v} = \widehat{v} \qquad \forall\, \widehat{v} \in \widehat{V}_r.$$

3.3 Construction of a global basis by reference mapping

Now we want to determine a global basis of the space V_h defined in (8) by means of the basis functions on the reference element. To this end, we define on each element $K \in \mathcal{T}_h$ the set of those global basis functions, which are non-zero on K. Using the basis on the reference element, we define at first the set of the nonconforming element-bubble functions $\phi_{K,\beta}$ with $\beta \in \mathcal{A}_{r-2}^{(d)}$ as

$$\phi_{K,\beta}(x) := \begin{cases} \widehat{\phi}_{\widehat{K},\beta}(F_K^{-1}(x)), & \forall x \in K, \\ 0, & \text{otherwise.} \end{cases} \tag{20}$$

Then, for each face $E \in \mathcal{E}_h$, we define the set of the corresponding face basis functions $\phi_{E,\alpha}$ with $\alpha \in \mathcal{A}_{r-1}^{(d-1)}$ on the two related elements $K(E)$ and $K'(E)$ (see Figure 3) as

$$\phi_{E,\alpha}(x) := \begin{cases} \widehat{\phi}_{\widehat{E},\alpha}(F_{K(E)}^{-1}(x)), & \text{if } x \in K(E),\ \widehat{E} := F_{K(E)}^{-1}(E), \\ s(\alpha')\widehat{\phi}_{\widehat{E}',\alpha'}(F_{K'(E)}^{-1}(x)), & \text{if } x \in K'(E),\ \widehat{E}' := F_{K'(E)}^{-1}(E), \\ 0, & \text{otherwise.} \end{cases} \tag{21}$$

Here $\widehat{E}$ denotes the reference face related to the original face E in the first element $K(E)$

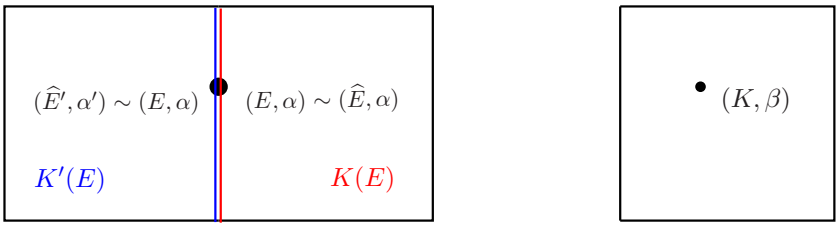

Figure 3: *Face node (E, α) (left) and element-bubble node (K, β) (right).*

adjacent to E and $\widehat{E}'$ the reference face of E in the second element $K'(E)$ adjacent to E. In the case of a boundary face $E \in \mathcal{E}_h^b$, there is no second element and we formally set $K'(E) = \emptyset$.

In (21), for a given inner face $E \in \mathcal{E}_h^i$ and a given multi-index $\alpha \in \mathcal{A}_{r-1}^{(d-1)}$, the multi-index $\alpha' \in \mathcal{A}_{r-1}^{(d-1)}$ and the sign $s(\alpha') \in \{-1,1\}$ are defined as follows. One can show that there exist a bijective mapping $\mu : \{1,\dots,d-1\} \to \{1,\dots,d-1\}$ and signs $s_k \in \{-1,1\}$, such that

$$F_{K(E)}\big(\widehat{T}_{\widehat{E}}(\xi)\big) = F_{K'(E)}\big(\widehat{T}_{\widehat{E}'}(\xi')\big) \qquad \forall \xi \in U_{d-1}, \tag{22}$$

where $\xi' = (\xi'_1,\dots,\xi'_{d-1}) \in U_{d-1}$ with $\xi'_k := s_k\,\xi_{\mu(k)}$ for $k = 1,\dots,d-1$. Then, we define

$$\alpha' = (\alpha'_k) := (\alpha_{\mu(k)}) \in \mathcal{A}_{r-1}^{(d-1)}, \qquad s(\alpha') := \prod_{k=1}^{d-1} (s_k)^{\alpha'_k} \in \{-1,+1\}. \tag{23}$$

For the implementation of the corresponding finite element method, the mapping μ and the signs s_k can be easily computed. In the two-dimensional case, the situation is very simple since

$$\alpha' = \alpha'_1 = \alpha_1 = \alpha \in \mathcal{A}_{r-1}^{(1)} = \{0,\dots,r-1\} \qquad \text{and} \qquad s(\alpha') = (-1)^{\alpha}.$$

It has been proven in [54] that the functions locally defined above form a basis, i.e., for the space V_h defined in (8), it holds

$$V_h = \operatorname{span}\big\{\phi_{E,\alpha} : E \in \mathcal{E}_h, \alpha \in \mathcal{A}_{r-1}^{(d-1)}\big\} \oplus \operatorname{span}\big\{\phi_{K,\beta} : K \in \mathcal{T}_h, \beta \in \mathcal{A}_{r-2}^{(d)}\big\}. \tag{24}$$

The representation (24) together with (20) and (21) shows that it is sufficient to compute the basis functions only once on the reference element and to use the reference mapping for the definition of the basis functions on the elements $K \in \mathcal{T}_h$. This is an advantage of the parametric version of the nonconforming elements.

Finally, we define the global interpolation operator $I_h : H^1(\Omega) \to V_h$ elementwisely for each $K \in \mathcal{T}_h$ by means of the reference mapping $F_K : \widehat{K} \to K$ and the operator $\widehat{\Pi}$ of § 3.2 as

$$I_h v\big|_K(x) := \widehat{\Pi}\big(v \circ F_K\big)\big(F_K^{-1}(x)\big) \qquad \forall\, x \in K. \tag{25}$$

Due to the construction of the nodal functionals, this formally discontinuous function $I_h v$ is really contained in V_h.

For multilevel grids, the parametric version of the nonconforming space V_h has optimal approximation properties. Since we have by construction that $\mathbb{P}_r(\widehat{K}) \subset \widehat{V}_r$, we can conclude from Theorem 9 in [53] the following error estimate.

Theorem 2. *Let $\{\mathcal{T}_h\}$ be a family of shape-regular multilevel grids generated from a coarse grid $\mathcal{T}^0$. Then, there exists a constant $C_2(\mathcal{T}^0)$ such that the local interpolation error estimate*

$$|v - I_h v|_{m,K} \le C_2(\mathcal{T}^0)\, h_K^{r+1-m} \|v\|_{r+1,K}, \qquad \forall v \in H^{r+1}(\Omega),$$

holds true for all $K \in \mathcal{T}_h$ and $m \in \{0,1\}$.

3.4 The $\widetilde{Q}_2$-element in two dimensions

As the "$\widetilde{Q}_r$-element" we will call the resulting nonconforming finite element constructed with the degree r. Here, the local polynomial space $\widehat{V}_2$ on the reference element $\widehat{K} = (-1,1)^2$ is the one defined in (15). Its dimension is 9, i.e., we need 9 nodal functionals to define the degrees of freedom. Let us denote by E_i, $i = 1,\ldots,4$, the faces of an element $K \in \mathcal{T}_h$ which are related to the reference faces $\widehat{E}_i$ of $\widehat{K}$, see Figure 4. We assume that these faces are numbered in a

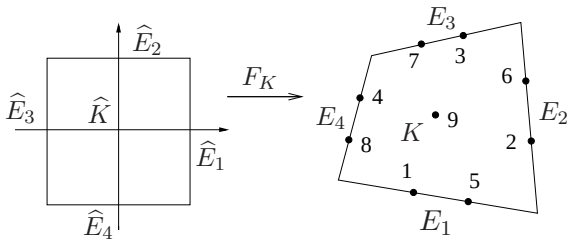

Figure 4: *Degrees of freedom of the $\widetilde{Q}_2$-element.*

counterclockwise sense. Let $\widehat{T}_i = \widehat{T}_{\widehat{E}_i} : (-1,1) \to \widehat{E}_i$ denote the affine parametrization of the reference face $\widehat{E}_i$ defined in Section 3.2 and oriented in a counterclockwise sense. Furthermore, we denote by $\widehat{v} : \widehat{K} \to \mathbb{R}$ the usual reference function associated with the original function $v : K \to \mathbb{R}$ by the relation $\widehat{v}(\hat{x}) := v(F_K^{-1}(\hat{x}))$ for all $\hat{x} \in \widehat{K}$. Using (11) and the fact that $L_0^{(1)}(\xi) = 1$ and $L_1^{(1)}(\xi) = \xi$, we get the following 8 nodal functionals associated with the faces of K

$$\begin{aligned} N_i^K(v) &:= \widehat{N}_i(\widehat{v}) := \widehat{N}_{\widehat{E}_i,0}(\widehat{v}) = |\widehat{E}_i|^{-1} \textstyle\int_{-1}^{1} \widehat{v}\big(\widehat{T}_i(\xi)\big)\, d\xi\,, \qquad i = 1,\ldots,4, \\ N_{4+i}^K(v) &:= \widehat{N}_{4+i}(\widehat{v}) := \widehat{N}_{\widehat{E}_i,1}(\widehat{v}) = |\widehat{E}_i|^{-1} \textstyle\int_{-1}^{1} \widehat{v}\big(\widehat{T}_i(\xi)\big)\xi\, d\xi\,, \qquad i = 1,\ldots,4. \end{aligned}$$

The last nodal functionals on K we get from (13) using $L_{(0,0)}^{(2)}(\hat{x}) = 1$

$$N_9^K(v) := \widehat{N}_9(\widehat{v}) := \widehat{N}_{\widehat{K},(0,0)}(\widehat{v}) = |\widehat{K}|^{-1} \int_{\widehat{K}} \widehat{v}(\hat{x})\, d\hat{x}\,.$$

To compute the basis functions $\widehat{\phi}_k$, $k = 1,\ldots,9$, on the reference element $\widehat{K}$ we choose basis polynomials $\widehat{p}_j$ as

$$\{\widehat{p}_1(\hat{x},\hat{y}),\ldots,\widehat{p}_9(\hat{x},\hat{y})\} := \{1,\hat{x},\hat{y},\hat{x}^2,\hat{x}\hat{y},\hat{y}^2,\hat{x}^2\hat{y},\hat{x}\hat{y}^2,\hat{x}^3\hat{y} - \hat{x}\hat{y}^3\} \tag{26}$$

and compute the coefficients $c_j^{(k)}$ in the $\widehat{\phi}_k$-ansatz

$$\widehat{\phi}_k(\hat{x},\hat{y}) = \sum_{j=1}^{9} c_j^{(k)} \widehat{p}_j(\hat{x},\hat{y}) \tag{27}$$

by solving the linear 9×9-system

$$\sum_{j=1}^{9} \widehat{N}_i(\widehat{p}_j) c_j^{(k)} = \delta_{i,j}, \qquad \forall\, i = 1, \ldots, 9. \tag{28}$$

In order to investigate the approximation properties of the $\widetilde{Q}_2$-element we have solved on the unit square $\Omega = (0,1)^2$ the Poisson problem with a prescribed smooth exact solution

$$u(x,y) = \sin(\pi x)\sin(\pi y)\,,$$

the right hand side $f = -\triangle u$ and corresponding Dirichlet boundary conditions. The grid $\mathcal{T}^\ell$ on level $\ell \geq 1$ was generated in a first step by applying ℓ recursive uniform refinements starting from the coarsest grid $\mathcal{T}^0$, which consists of just one element $K = \Omega$. In a second step this multilevel grid was modified by a stochastical perturbation of the vertices of the grid with a size of 1% until 20% of the mesh size h, see Figure 5.

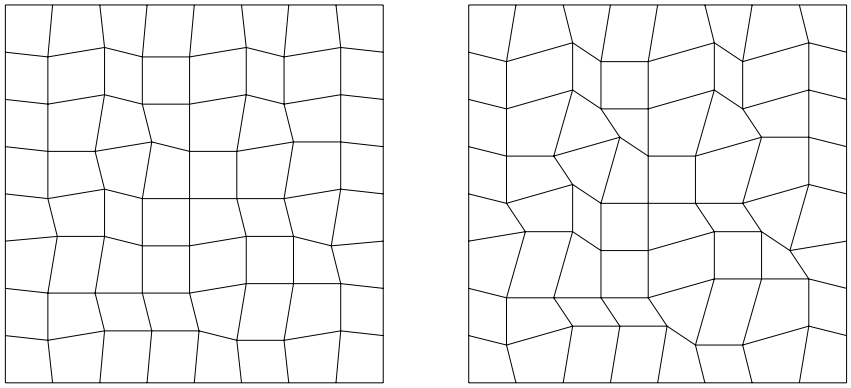

Figure 5: Grids on level $\ell = 3$ which are stochastically deformed with 10% (left) and 20% (right).

Table 1 shows that the $\widetilde{Q}_2$-element works well on slightly perturbed (shape-regular) multilevel grids (perturbation $< 5\%$) but it loses its optimal order of $\mathcal{O}(h^3)$ in the L^2-norm and $\mathcal{O}(h^2)$ in the H^1-norm on significantly perturbed grids (perturbation $\geq 5\%$).

The reason for this reduction in the order of approximation of the nonconforming $\widetilde{Q}_r$-element is the fact that for a non-affine reference mapping $F_K : \widehat{K} \to K$, which occurs on general shape-regular meshes, the restriction $V_r(K)$ of the finite element space V_h to an element $K \in \mathcal{T}_h$, defined in (2), does not contain the polynomial space $\mathbb{P}_r(K)$ in real coordinates. However, it has been shown in [5] that the condition $\mathbb{P}_r(K) \subset V_r(K)$ is necessary for optimal order of approximation.

	1% deformation		5% deformation		10% deformation		20% deformation	
level	L2-error	factor	L2-error	factor	L2-error	factor	L2-error	factor
2	1.61E-02		1.63E-02		1.66E-02		1.81E-02	
3	2.07E-03	7.79	2.17E-03	7.49	2.39E-03	6.96	3.19E-03	5.66
4	2.58E-04	8.02	2.69E-04	8.06	3.09E-04	7.75	5.01E-04	6.38
5	3.23E-05	7.99	3.41E-05	7.90	4.04E-05	7.65	7.32E-05	6.84
6	4.04E-06	8.00	4.29E-06	7.94	5.44E-06	7.43	1.28E-05	5.72
7	5.05E-07	8.00	5.52E-07	7.78	8.45E-07	6.43	2.78E-06	4.60
8	6.31E-08	8.00	7.52E-08	7.34	1.62E-07	5.22	6.58E-07	4.23
9	7.90E-09	7.99	1.21E-08	6.22	3.71E-08	4.36	1.64E-07	4.01
	H1-error	factor	H1-error	factor	H1-error	factor	H1-error	factor
2	2.27E-01		2.28E-01		2.30E-01		2.39E-01	
3	5.60E-02	4.06	5.80E-02	3.94	6.22E-02	3.71	7.67E-02	3.12
4	1.38E-02	4.04	1.43E-02	4.05	1.60E-02	3.88	2.51E-02	3.06
5	3.46E-03	4.00	3.61E-03	3.97	4.23E-03	3.79	8.08E-03	3.10
6	8.63E-04	4.00	9.19E-04	3.93	1.26E-03	3.35	3.55E-03	2.28
7	2.16E-04	4.00	2.45E-04	3.75	4.67E-04	2.70	1.72E-03	2.07
8	5.40E-05	4.00	7.42E-05	3.31	2.06E-04	2.27	8.43E-04	2.04
9	1.35E-05	3.99	2.82E-05	2.63	1.00E-04	2.05	4.24E-04	1.99

Table 1: Discretization error $u - u_h$ of the $\widetilde{Q}_2$-element in the L^2-norm and the H^1-norm on multilevel grids with stochastical deformation.

4 Robust approximation by a nonparametric version

The idea of the nonparametric version of nonconforming elements, see [60], is to choose on each element such shape functions which are polynomial in the real coordinates. This ensures the condition $\mathbb{P}_r(K) \subset V_r(K)$ of [5] for optimal approximation. The way to obtain polynomial shape functions in the real coordinates is to work with an affine mapping $\widetilde{F}_K : \widehat{K} \to K$

$$\widetilde{F}_K(\hat{x}) := c_K + B_K \hat{x} \qquad \forall \hat{x} \in \widehat{K}, \tag{29}$$

which is a linearization of the usual reference mapping $F_K : (-1,1)^d \to K$ with the constant vector $c_K := F_K(0)$, the Jacobi matrix $B_K := DF_K(0)$ and the variable K-dependent reference element $\widehat{K} := \widetilde{F}_K^{-1}(K)$. The vector c_K is the barycenter of the element K and the column vectors of the matrix B_K are $b_K^j := c_j - c_K$, $j = 1, \ldots, d$, where c_j is the barycenter of an associated face E_j of K, see Figure 6. The coordinates $\hat{x}_j$, $j = 1, \ldots, d$, of $\hat{x} \in \widehat{K}$ can be regarded as the local coordinates of the real world coordinates x_j of a point $x = (x_j) \in K$

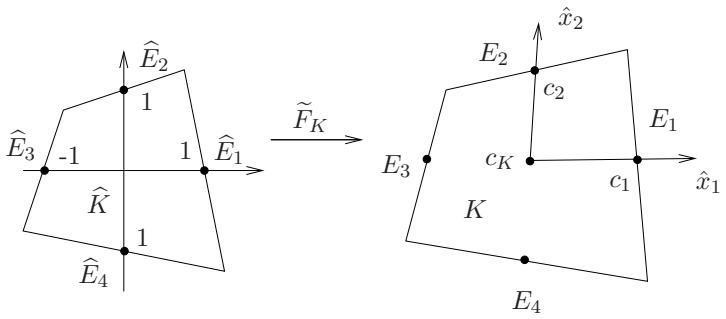

Figure 6: *Affine reference mapping* $\widetilde{F}_K : \widehat{K} \to K$.

with

$$x = \widetilde{F}_K(\hat{x}) = c_K + b_K^1 \hat{x}_1 + \ldots + b_K^d \hat{x}_d.$$

Thus, for functions $\widehat{v} : \widehat{K} \to \mathbb{R}$, which are polynomial in the coordinates $\hat{x}_j$, the corresponding function $v : K \to \mathbb{R}$ with $v(x) := \widehat{v}(\hat{x})$ is also polynomial in the real world coordinates x_j of $x \in K$. Moreover, the condition $\mathbb{P}_r(K) \subset V_r(K)$ for optimal approximation properties is satisfied if the local space $\widehat{V}_r$ on the reference element satisfies the condition $\mathbb{P}_r(\widehat{K}) \subset \widehat{V}_r$. So, in the nonparametric version of nonconfoming elements, we formally also work with a reference mapping $\widetilde{F}_K$, but this mapping is affine in contrast to the usual mapping F_K of the parametric version. For the special case that an element is a parallelogram or a parallelepiped, both versions are identical since here the usual multilinear reference mappping F_K is affine.

In the following, we will describe the definition of the basis functions for the nonparametric version. At first we choose polynomial basis functions $\widehat{p}_j : \widehat{K} \to \mathbb{R}$ for the local approximation space $\widehat{V}_r$ on the reference element $\widehat{K} := \widetilde{F}_K^{-1}(K)$ such that

$$\widehat{V}_r := \operatorname{span}\{\widehat{p}_j : \ j = 1, \ldots, m\}. \tag{30}$$

For the case $r = 2$, we would use the same polymonials as in (26) for the parametric version. The basis function $\widehat{\phi}_k \in \widehat{V}_r$ is computed as a linear combination of the polynomials $\widehat{p}_j$ with coefficients $c_j^{(k)}$

$$\widehat{\phi}_k(\hat{x}) = \sum_{j=1}^{m} c_j^{(k)} \widehat{p}_j(\hat{x}) \qquad \forall\, \hat{x} \in \widehat{K}. \tag{31}$$

These m coefficients are determined by the m conditions

$$\widehat{N}_i(\widehat{\phi}_k) = \delta_{i,k} \qquad \forall\, i = 1, \ldots, m.$$

The difference to the parametric version is that the nodal functionals $\widehat{N}_i$ depend on K, i.e., they change when the element K is changing. For a given face $\widehat{E}$ of $\widehat{K}$ and a multiindex

$\alpha \in \mathcal{A}_{r-1}^{(d-1)}$, the associated nodal functional is defined by an integral over the related original face $E = \widetilde{F}_K(\widehat{E})$, i.e.

$$\widehat{N}_{\widehat{E},\alpha}(\widehat{v}) := |E|^{-1} \int_E v(x) L_\alpha^{(d-1)}\big(\xi_E(x)\big)\, dE, \tag{32}$$

where $\xi = \xi_E(x) \in U_{d-1}$ denotes the parameter value associated to $x \in E$ such that $x = T_E(\xi)$ with the mapping $T_E : U_{d-1} \to E$ defined in (7) for the parametric version. For $\widehat{K} = \widetilde{F}_K^{-1}(K)$ and a multiindex $\beta \in \mathcal{A}_{r-2}^{(d)}$, the associated nodal functional is defined by an integral over the original element K, i.e.

$$\widehat{N}_{\widehat{K},\beta}(\widehat{v}) := |K|^{-1} \int_K v(x) L_\beta^{(d)}\big(F_K^{-1}(x)\big)\, dK. \tag{33}$$

The K-dependent set $\widehat{\mathcal{N}}_r$ of nodal functionals related to $\widehat{K}$ is then

$$\widehat{\mathcal{N}}_r = \{\widehat{N}_i : i = 1, \dots, m\} = \big\{\widehat{N}_{\widehat{E},\alpha} : \widehat{E} \in \widehat{\mathcal{E}}, \alpha \in \mathcal{A}_{r-1}^{(d-1)}\big\} \cup \big\{\widehat{N}_{\widehat{K},\beta} : \beta \in \mathcal{A}_{r-2}^{(d)}\big\}.$$

In the nonparametric version, the computational costs to determine the local basis functions for an element $K \in \mathcal{T}_h$ are:

- compute the matrix $N \in \mathbb{R}^{m\times m}$ with the entries $N_{i,j} = \widehat{N}_i(\widehat{p}_j)$ by applying corresponding Gaussian integration formulas to (32) and (33).
- compute the matrix of coefficients $C \in \mathbb{R}^{m\times m}$ with the entries $C_{i,j} = c_i^{(j)}$ for the basis functions $\widehat{\phi}_k$ defined in (31) by $C = N^{-1}$.
- evaluate the basis functions $\widehat{\phi}_k$, $k = 1, \dots, m$, at all Gaussian integration points $\hat{x}^{(j)} \in \widehat{K} = \widetilde{F}_K^{-1}(K)$ for assembling the local element matrix and right hand side vector of the discretization.

In the parametric version, since the reference element $\widehat{K} = (-1, 1)^d$ is fixed here for all elements $K \in \mathcal{T}_h$, the local basis functions $\widehat{\phi}_k$ as well as the Gaussian integration points on $\widehat{K}$ do not change for different elements such that the values of the basis functions at the integration points can be precomputed before starting the assembling process. Thus, the increased computational costs of the nonparametric version are a disadvantage compared to the parametric version. The main advantage of nonparametric elements is that they guarantee optimal approximation properties for general shape-regualr meshes. This will be shown in Table 3 below. In the following, we will call the nonparametric nonconforming finite element of degree r as the "$\widetilde{Q}_r^n$-*element*".

5 Robust approximation by nonconforming bubble functions

Our aim is, on the one hand, to use the parametric version due to its lower computational costs and, on the other hand, to avoid the reduction in the order of approximation on general shape-regular grids. The following idea seems to be a good compromise to achieve both. We add on each element one ore more nonconforming bubble functions such that the polynomial space $\mathbb{Q}_r(\widehat{K})$ is a subspace of the local approximation space $\widehat{V}_r$ on the reference element. Then, the resulting nonconforming finite element space V_h contains as a subspace the global conforming $\mathbb{Q}_r$ space which guarantees optimal approximation properties on general shape-regular meshes. The additional computational costs are relatively small since the nonconforming bubble functions can be eliminated during the assembling process by static condensation. We will call the resulting nonconforming finite element as the "$\widetilde{Q}_r^b$*-element*".

5.1 The $\widetilde{Q}_2^b$-element in the 2D-case

In the two-dimensional case with $r = 2$, we only need one additional nonconforming bubble function. In order to achieve the property $\mathbb{Q}_2(\widehat{K}) \subset \widehat{V}_2^b$ we add to the space $\widehat{V}_2$ of the $\widetilde{Q}_2$-element the polynomial $\widehat{p}_{10}(\hat{x}, \hat{y}) = \hat{x}^2\hat{y}^2$ such that

$$\widehat{V}_2^b := \mathbb{P}_2(\widehat{K}) \oplus \operatorname{span}\{\hat{x}^2\hat{y}, \hat{x}\hat{y}^2, \hat{x}^2\hat{y}^2, \hat{x}^3\hat{y} - \hat{x}\hat{y}^3\} = \operatorname{span}\{\widehat{p}_1, \ldots, \widehat{p}_{10}\}. \tag{34}$$

As the basis functions $\widehat{\phi}_k$ of $\widehat{V}_2$ we choose the basis functions $\widehat{\phi}_1, \ldots, \widehat{\phi}_9$ of the parametric $\widetilde{Q}_2$-element and the function $\widehat{\phi}_{10}$ defined by

$$\widehat{\phi}_{10}(\hat{x}, \hat{y}) := \widehat{p}_{10}(\hat{x}, \hat{y}) - \sum_{j=1}^{9} \widehat{N}_j(\widehat{p}_{10})\widehat{\phi}_j(\hat{x}, \hat{y}).$$

Obviously, it holds $\widehat{N}_i(\widehat{\phi}_{10}) = 0$ for all $i = 1, \ldots, 9$, such that the function $\widehat{\phi}_{10}$ is a nonconforming bubble function since it is zero in an intgral sense on the boundary faces of $\widehat{K}$. Therefore, the additional nonconforming bubble functions do not reduce the order of the consistency error.

The following numerical results confirm that the new $\widetilde{Q}_2^b$-element has optimal approximation properties on general shape-regular grids. The test problem is the same as for Table 1. Table 2 shows that the $\widetilde{Q}_2^b$-element works well with optimal order of $\mathcal{O}(h^3)$ in the L^2-norm and $\mathcal{O}(h^2)$ in the H^1-norm on all considered grids. For a grid deformation of 20%, Table 3 presents the discretization errors in the L^2-norm for the Q_2-element, the parametric nonconforming $\widetilde{Q}_2$-element, the new $\widetilde{Q}_2^b$-element and the nonparametric $\widetilde{Q}_2^n$-element. Except for the $\widetilde{Q}_2$-element, all elements have nearly the same optimal approximation properties. Table 4 shows the analogous results for the H^1-norm.

	1% deformation		5% deformation		10% deformation		20% deformation	
level	L2-error	factor	L2-error	factor	L2-error	factor	L2-error	factor
2	1.61E-02		1.62E-02		1.66E-02		1.80E-02	
3	2.07E-03	7.77	2.17E-03	7.48	2.39E-03	6.96	3.17E-03	5.69
4	2.58E-04	8.02	2.69E-04	8.07	3.05E-04	7.82	4.68E-04	6.78
5	3.23E-05	7.99	3.40E-05	7.91	3.95E-05	7.73	6.37E-05	7.35
6	4.04E-06	8.00	4.25E-06	7.99	4.95E-06	7.98	7.93E-06	8.02
7	5.05E-07	8.00	5.33E-07	7.98	6.23E-07	7.94	1.01E-06	7.85
8	6.31E-08	8.00	6.67E-08	7.99	7.81E-08	7.97	1.27E-07	7.93
9	7.89E-09	8.00	8.34E-09	7.99	9.79E-09	7.98	1.60E-08	7.95
	H1-error	factor	H1-error	factor	H1-error	factor	H1-error	factor
2	2.26E-01		2.27E-01		2.30E-01		2.40E-01	
3	5.59E-02	4.04	5.79E-02	3.92	6.20E-02	3.70	7.62E-02	3.15
4	1.38E-02	4.04	1.43E-02	4.05	1.57E-02	3.96	2.12E-02	3.58
5	3.46E-03	4.00	3.59E-03	3.98	3.99E-03	3.93	5.59E-03	3.80
6	8.63E-04	4.00	8.98E-04	4.00	1.00E-03	3.98	1.41E-03	3.95
7	2.16E-04	4.00	2.25E-04	3.99	2.52E-04	3.98	3.57E-04	3.95
8	5.40E-05	4.00	5.62E-05	4.00	6.32E-05	3.99	9.00E-05	3.97
9	1.35E-05	4.00	1.41E-05	4.00	1.58E-05	3.99	2.26E-05	3.98

Table 2: Approximation properties of the new $\widetilde{Q}_2^b$-element.

	Q_2		$\widetilde{Q}_2$		$\widetilde{Q}_2^b$		$\widetilde{Q}_2^n$	
level	L2	factor	L2	factor	L2	factor	L2	factor
2	1.68E-02		1.80E-02		1.80E-02		1.75E-02	
3	3.03E-03	5.5457	3.19E-03	5.6602	3.17E-03	5.6895	3.00E-03	5.8454
4	4.42E-04	6.8580	5.00E-04	6.3787	4.67E-04	6.7802	4.38E-04	6.8514
5	6.07E-05	7.2860	7.31E-05	6.8421	6.36E-05	7.3470	6.02E-05	7.2851
6	7.54E-06	8.0525	1.28E-05	5.7177	7.93E-06	8.0236	7.40E-06	8.1254
7	9.58E-07	7.8659	2.78E-06	4.6028	1.01E-06	7.8532	9.45E-07	7.8347
8	1.20E-07	7.9327	6.57E-07	4.2301	1.27E-07	7.9334	1.19E-07	7.9440
9	1.52E-08	7.9433	1.63E-07	4.0138	1.60E-08	7.9535	1.49E-08	7.9455
10	1.89E-09	8.0218	4.11E-08	3.9773	1.99E-09	8.0144	1.86E-09	8.0382

Table 3: L^2-errors and error reduction factors with respect to the previous grid level on grids with 20% deformation.

	Q_2		$\widetilde{Q}_2$		$\widetilde{Q}_2^b$		$\widetilde{Q}_2^n$	
level	H1	factor	H1	factor	H1	factor	H1	factor
2	2.18E-01		2.39E-01		2.39E-01		2.40E-01	
3	7.16E-02	3.0553	7.66E-02	3.1177	7.61E-02	3.1504	7.30E-02	3.2866
4	1.99E-02	3.5895	2.50E-02	3.0599	2.12E-02	3.5847	2.00E-02	3.6394
5	5.27E-03	3.7843	8.07E-03	3.1019	5.58E-03	3.8034	5.29E-03	3.7885
6	1.33E-03	3.9527	3.54E-03	2.2782	1.41E-03	3.9519	1.33E-03	3.9814
7	3.37E-04	3.9529	1.71E-03	2.0672	3.57E-04	3.9540	3.36E-04	3.9511
8	8.50E-05	3.9719	8.42E-04	2.0356	8.99E-05	3.9723	8.46E-05	3.9778
9	2.13E-05	3.9822	4.23E-04	1.9880	2.25E-05	3.9843	2.12E-05	3.9819
10	5.33E-06	3.9988	2.13E-04	1.9830	5.65E-06	3.9961	5.30E-06	4.0047

Table 4: H^1-errors and error reduction factors with respect to the previous grid level on grids with 20% deformation.

5.2 Error analysis

For simplicity of the presentation, we restrict the analysis to the two-dimensional Poisson equation: *Find* $u : \Omega \to \mathbb{R}$ *such that*

$$\begin{aligned} -\triangle u &= f \qquad \text{in } \Omega, \\ u &= 0 \qquad \text{on } \partial\Omega, \end{aligned} \tag{35}$$

where $\Omega \subset \mathbb{R}^2$ is a domain with polygonal boundary and $f \in L^2(\Omega)$ a given function. The weak formulation of this problem reads: *Find* $u \in H_0^1(\Omega)$ *such that*

$$a(u,v) := (\nabla u, \nabla v)_\Omega = (f,v)_\Omega \qquad \forall v \in H_0^1(\Omega). \tag{36}$$

On the space $H^{1,h}(\Omega)$ defined in (3), we introduce the seminorm

$$|v|_{1,h} := \Big(\sum_{K \in \mathcal{T}_h} |v|_{1,K}^2 \Big)^{1/2} \tag{37}$$

and the discrete version of the bilinear form $a(\cdot,\cdot)$

$$a_h(u,v) := \sum_{K \in \mathcal{T}_h} (\nabla u, \nabla v)_K \qquad \forall u, v \in H^{1,h}(\Omega). \tag{38}$$

Let V_h be the finite element space related to the $\widetilde{Q}_r^b$-element and $V_{0,h}$ the subspace with discrete homogeneous boundary conditions defined by (10) with $g = 0$. Then, the discrete problem reads: *Find* $u_h \in V_{0,h}$ *such that*

$$a_h(u_h, v_h) = (f,v)_\Omega \qquad \forall v_h \in V_{0,h}. \tag{39}$$

The new nonconforming $\widetilde{Q}_r^b$-element has the following approximation properties.

Lemma 3. *Let $\{\mathcal{T}_h\}$ be a family of shape-regular grids and V_h the finite element space of the nonconforming $\widetilde{Q}_r^b$-element which is defined by (8) with the local space $V_h(K)$ derived by (2) from a reference space $\widehat{V}_r$ of some order $r \geq 1$ such that $\mathbb{Q}_r(\widehat{K}) \subset \widehat{V}_r$. Then, there exists an interpolation operator $I_h : H^2(\Omega) \to V_h$ such that the local estimate of the approximation error*

$$|v - I_h v|_{m,K} \leq C\, h_K^{r+1-m} |v|_{r+1,K}, \qquad \forall v \in H^{r+1}(\Omega), \tag{40}$$

holds true for all $K \in \mathcal{T}_h$ and $m \in \{0, 1\}$. Moreover, for a function $v \in H^2(\Omega) \cap H_0^1(\Omega)$, it holds $I_h v \in V_{0,h}$.

Proof. Let $v \in H^{r+1}(\Omega)$ be given and $I_h v \in C(\overline{\Omega})$ the standard interpolate of the function v in the classical conforming finite element space of type $\mathbb{Q}_r$. Then, with the reference mapping $F_K : \widehat{K} \to K$ it holds

$$I_h v|_K \circ F_K \in \mathbb{Q}_r(\widehat{K}) \subset \widehat{V}_r.$$

Since $I_h v$ is continuous, the compatibility property (6) is satisfied for $I_h v$. Due to (8), this implies $I_h v \in V_h$. The estimate (40) follows from the well known approximation properties of the conforming finite element space of type $\mathbb{Q}_r$. For a function $v \in H^2(\Omega) \cap H_0^1(\Omega)$, the conforming interpolate $I_h v$ is zero at the boundary of Ω which implies $I_h v \in V_{0,h}$. □

In the following, we prove an optimal estimate of the discretization error in the broken energy norm $|\cdot|_{1,h}$. Note that the seminorm defined in (37) is a norm on the subspace $V_{0,h}$.

Theorem 4. *Let $\{\mathcal{T}_h\}$ be a family of shape-regular grids and $V_{0,h}$ the finite element space of the nonconforming $\widetilde{Q}_r^b$-element with discrete homogeneous boundary conditions where $r \geq 1$. Assume that the solution $u \in H_0^1(\Omega)$ of problem (36) has the regularity property $u \in H^{r+1}(\Omega)$. Then, the solution $u_h \in V_{0,h}$ of the discrete problem (39) satisfies the error estimate*

$$|u - u_h|_{1,\Omega} \leq C\, h^r |u|_{r+1,\Omega}. \tag{41}$$

Proof. Let $I_h u \in V_{0,h}$ be the interpolate from Lemma 3 and $v_h := I_h u - u_h \in V_{0,h}$. Then we have

$$|v_h|_{1,h}^2 = a_h(v_h, v_h) = \underbrace{a_h(u, v_h) - (f, v_h)_\Omega}_{=:\, e(u, v_h)} + a_h(I_h u - u, v_h). \tag{42}$$

In the following, we will estimate the consistency error functional $e(u, \cdot)$. Partial integration yields

$$e(u, v_h) = \sum_{K \in \mathcal{T}_h} \sum_{E \in \mathcal{E}(K)} \big\langle\, n_E^K \cdot \nabla u, v_h \,\big\rangle_E = \sum_{E \in \mathcal{E}_h} \underbrace{\big\langle\, n_E \cdot \nabla u, [v_h]_E \,\big\rangle_E}_{=:\, e_E(u, v_h)}$$

where, for boundary edges $E \in \mathcal{E}_h^b$, we define $[v_h]_E(x) := v_h|_{K(E)}(x)$ for all $x \in E$. In our two-dimensional case, the new compatibility condition (6) is equivalent to the usual one in (5), i.e., we have

$$\int_E q\,[v_h]_E\,d\gamma = 0 \qquad \forall E \in \mathcal{E}_h\ \forall q \in \mathbb{P}_{r-1}(E). \tag{43}$$

In order to estimate $e_E(u, v_h)$ we define on element $K(E)$ the polynomial $q \in \mathbb{P}_{r-1}(K(E))$ as the local L^2-projection of the function $w := n_E \cdot \nabla u$. Then, the compatibility condition (43) yields

$$e_E(u, v_h) = \langle\, w - q, [v_h]_E \,\rangle_E \le \|w - q\|_{0,E}\, \|\,[v_h]_E\,\|_{0,E}.$$

Let $K \in \mathcal{T}_h$ be an element with the edge E. By standard arguments, like transformation to the reference element $\widehat{K}$, trace theorem on $\widehat{K}$ and back-transformation, we get the estimate

$$\|v\|_{0,E} \le Ch_K^{1/2}|v|_{1,K} + Ch_K^{-1/2}\|v\|_{0,K} \qquad \forall v \in H^1(K). \tag{44}$$

This implies by means of standard interpolation estimates for the L^2-projection

$$\|w - q\|_{0,E} \le Ch_K^{1/2}|w - q|_{1,K(E)} + Ch_K^{-1/2}\|w - q\|_{0,K(E)} \le Ch^{r-1/2}|u|_{r+1,K(E)}.$$

Let v_E denote the trace of the local function $v_h|_{K(E)}$ on edge E and, for an inner edge E, v'_E the trace of $v_h|_{K'(E)}$ on E. For the integral mean value c_E of v_E, it holds due to (43)

$$c_E := |E|^{-1}\int_E v_E\,d\gamma = |E|^{-1}\int_E v'_E\,d\gamma.$$

Standard estimates for the constant mean value approximation together with (44) yield

$$\|v_E - c_E\|_{0,E} \le Ch^{1/2}|v_h|_{1,K(E)} \qquad \text{and} \qquad \|v'_E - c_E\|_{0,E} \le Ch^{1/2}|v_h|_{1,K'(E)}$$

such that

$$\|\,[v_h]_E\,\|_{0,E} \le \|v_E - c_E\|_{0,E} + \|v'_E - c_E\|_{0,E} \le Ch^{1/2}\big(|v_h|_{1,K(E)} + |v_h|_{1,K'(E)}\big).$$

In the case of a boundary edge $E \in \mathcal{E}_h^b$, we assume that $K'(E)$ is the empty set. Thus, we obtain

$$|e_E(u, v_h)| \le Ch^r|u|_{r+1,K(E)}\big(|v_h|_{1,K(E)} + |v_h|_{1,K'(E)}\big).$$

If we take the sum over all edges $E \in \mathcal{E}_h$ and apply the Cauchy-Schwarz inequality we get

$$|e(u, v_h)| \le Ch^r\,|u|_{r+1,\Omega}\,|v_h|_{1,h}.$$

The last term in (42) can be estimated by means of Lemma 3 as

$$a_h(I_h u - u, v_h) \le \sum_{K\in\mathcal{T}_h} Ch_K^r|u|_{r+1,K}\,|v_h|_{1,K} \le Ch^r|u|_{r+1,\Omega}\,|v_h|_{1,h}$$

which implies for $v_h = I_h u - u_h$

$$|v_h|_{1,h} \leq Ch^r |u|_{r+1,\Omega}.$$

Using the triangle inequality, we finally obtain $|u-u_h|_{1,h} \leq |u-I_h u|_{1,h} + |v_h|_{1,h} \leq Ch^r |u|_{r+1,\Omega}$. □

Let us note that, for a convex domain Ω, we can prove by means of the well-known duality argument the following optimal L^2-norm estimate

$$\|u - u_h\|_{0,\Omega} \leq Ch^{r+1} |u|_{r+1,\Omega}. \tag{45}$$

6 Multigrid solver for higher order elements

In addition to the good numerical robustness w.r.t. mesh deformation, the proposed higher order elements admit the application of efficient multigrid solvers, too. In the following, we shortly discuss the multigrid behaviour and provide convergence results for corresponding Poisson problems with given analytical solutions and homogeneous Dirichlet boundary conditions, on the unit square as well as on a more complex 'flow around cylinder' configuration (Fig. 7) which will be the basis for the subsequent Navier-Stokes calculations. The resulting hierarchies of finer meshes are again recursively obtained by connecting opposite midpoints on the coarser level. If elements at a curved boundary part are refined, the new vertices are moved to the boundary. The subsequent results for solving the Poisson problems, discretized

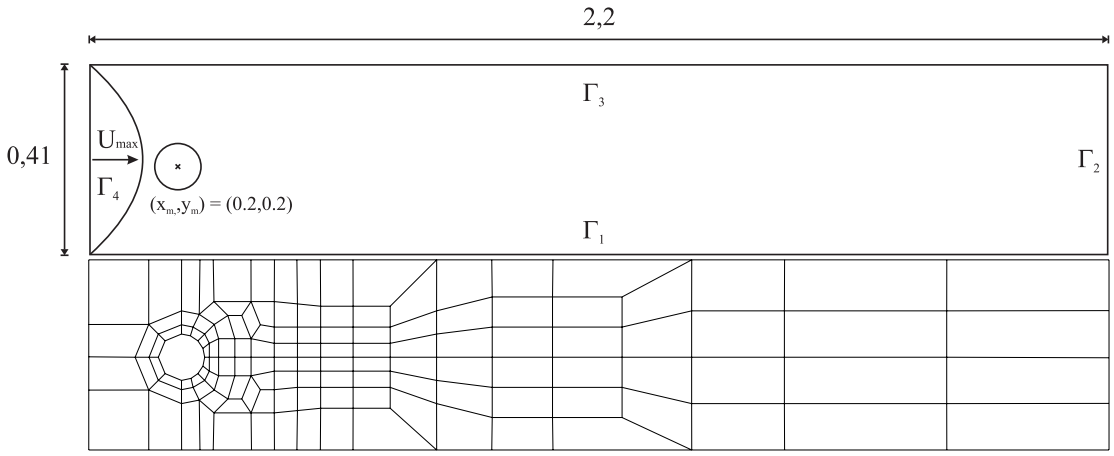

Figure 7: Geometry and coarse grid (level 1) for the 'flow around cylinder' configuration.

with $\widetilde{Q}_2$- and $\widetilde{Q}_2^b$-elements, on the unit square (see Table 5) as well as on the 'channel geometry' (see Table 6) show the resulting multigrid iteration steps (MG-Iter) and the convergence rates (MG-Rho) for different refinement levels to gain 5 digits. We apply a standard geometrical multigrid approach which uses the corresponding full order finite element interpolate for

the prolongation (see [43]) and the transposed matrix for the restriction operator. The results show the expected level-independent convergence behaviour in Table 5 and 6. Moreover, we demonstrate the corresponding convergence behaviour for different standard smoothing operators in Table 7 for the more complex 'flow around cylinder' configuration which illustrates the well-known superior convergence behaviour of ILU-type smoothers.

$\widetilde{Q}_2$ (without bubble)				
	V-cycle		F-cycle	
Level	MG-Iter	MG-Rho	MG-Iter	MG-Rho
4	5	8.187E-02	5	7.847E-02
5	5	9.917E-02	5	7.405E-02
6	6	1.137E-01	5	7.196E-02
7	6	1.192E-01	5	7.169E-02
8	6	1.229E-01	5	7.166E-02
9	6	1.258E-01	5	7.165E-02
10	6	1.280E-01	5	7.165E-02

$\widetilde{Q}_2^b$ (with bubble)				
	V-cycle		F-cycle	
Level	MG-Iter	MG-Rho	MG-Iter	MG-Rho
4	5	8.328E-02	5	7.584E-02
5	5	9.944E-02	5	7.984E-02
6	6	1.125E-01	5	8.027E-02
7	6	1.179E-01	5	8.032E-02
8	6	1.216E-01	5	8.033E-02
9	6	1.245E-01	5	8.033E-02
10	6	1.267E-01	5	8.033E-02

Table 5: Multigrid convergence (with 2 SOR smoothing steps) on the unit square.

Currently, we are extending the ideas in [43], where optimal (superlinear) convergence of multigrid solvers for conforming quadratic FEM has been shown, to the case of the proposed nonconforming higher order elements. The corresponding theoretical and numerical analysis w.r.t. optimal grid transfer operators and the use of adaptive step-lenght-correction of the coarse grid solutions (which is standard for nonconforming FEM) together with numerical studies of the resulting convergence behaviour on much more complex domains and computational meshes will be the subject of a forthcoming paper.

$\widetilde{Q}_2$ (without bubble)				
	V-cycle		F-cycle	
Level	MG-Iter	MG-Rho	MG-Iter	MG-Rho
3	13	4,071E-01	13	4,074E-01
4	13	4,042E-01	13	4,025E-01
5	13	4,016E-01	12	3,773E-01
6	13	4,046E-01	11	3,477E-01
7	13	4,057E-01	11	3,317E-01

$\widetilde{Q}_2^b$ (with bubble)				
	V-cycle		F-cycle	
Level	MG-Iter	MG-Rho	MG-Iter	MG-Rho
3	13	4,071E-01	13	4,074E-01
4	13	4,042E-01	13	4,025E-01
5	13	4,014E-01	12	3,773E-01
6	13	4,043E-01	11	3,477E-01
7	13	4,054E-01	11	3,317E-01

Table 6: Multigrid convergence (with 2 SOR smoothing steps) on the 'flow around cylinder' configuration.

	Jacobi		SOR		ILU(0)	
Level	MG-Iter	MG-Rho	MG-Iter	MG-Rho	MG-Iter	MG-Rho
2	26	6.406E-01	13	3.934E-01	4	2.801E-02
3	30	6.763E-01	14	4.331E-01	5	5.852E-02
4	29	6.706E-01	14	4.283E-01	4	5.605E-02
5	27	6.526E-01	13	4.044E-01	4	5.540E-02
6	25	6.298E-01	12	3.755E-01	4	5.448E-02
7	23	6.035E-01	11	3.441E-01	5	6.694E-02

Table 7: Multigrid behaviour for the Poisson problem with $\widetilde{Q}_2^b$-elements for different smoothing operators (2 smoothing steps) on the 'flow around cylinder' configuration.

7 Application to incompressible flow problems

Finally, we demonstrate the high potential of these new nonconforming finite elements for the simulation of incompressible flow problems which due to the well-known LBB-condition require special finite element pairs for discretizing velocity and pressure. As explanined in the introduction, discontinuous pressure approximations together with edge, resp., face-oriented velocity ansatz spaces promise some advantageous behaviour regarding efficient solvers, particularly for highly nonstationary flows.

As a first test case, we consider the standard 'flow around cylinder' benchmark at Reynolds number Re=20 (see [73] for the details) with the computational meshes of the previous section. Here, we use the nonconforming $\widetilde{Q}_2$-elements for the velocity, and discontinuous, piecewise linear elements ($\mathbb{P}_1^{dc}$) for the pressure approximations. Table 8 shows the typical multigrid behaviour for solving the resulting Oseen equations inside of an outer fixed-point iteration which is based on the Vanka smoother (see [70, 72]). Table 9 provides the corresponding results for the drag and lift values as essential quantities of the underlying benchmarking configuration. It clearly shows the high order accuracy of these new finite elements.

$\widetilde{Q}_2$ / $\mathbb{P}_1^{dc}$				
	V-cycle		F-cycle	
level	MG-Iter	MG-Rho	MG-Iter	MG-Rho
2	5	8,022E-02	5	8,022E-02
3	6	1,209E-01	5	9,486E-02
4	7	1,651E-01	5	8,852E-02
5	8	2,181E-01	5	8,195E-02

$\widetilde{Q}_2^b$ / $\mathbb{P}_1^{dc}$				
	V-cycle		F-cycle	
level	MG-Iter	MG-Rho	MG-Iter	MG-Rho
2	5	8,041E-02	5	8,041E-02
3	6	1,212E-01	5	9,514E-02
4	7	1,655E-01	5	8,858E-02
5	8	2,186E-01	5	8,203E-02

Table 8: Multigrid iterations and convergence rates (4 smoothing steps with the Vanka smoother) for the Oseen equations on the 'flow around cylinder' geometry.

	$\widetilde{Q}_1$ / $\mathbb{P}_0^{dc}$		$\widetilde{Q}_2^b$ / $\mathbb{P}_1^{dc}$		Q_2 / $\mathbb{P}_1^{dc}$	
level	drag	lift	drag	lift	drag	lift
1	1.97E-01	2.13E-00	4.19E-02	7.93E-01	4.45E-02	5.47E-01
2	3.88E-02	4.19E-01	7.72E-03	2.14E-01	1.42E-02	1.51E-01
3	4.51E-03	2.15E-01	3.14E-03	4.27E-02	3.92E-03	1.82E-02
4	3.39E-03	1.18E-01	8.63E-04	1.07E-02	9.92E-04	5.12E-03
5	2.17E-03	5.46E-02	-	-	-	-
6	1.25E-03	2.36E-02	-	-	-	-
7	6.82E-04	1.02E-02	-	-	-	-

Table 9: Relative errors for the drag and lift values w.r.t. the reference values 'drag(ref)' $\approx$ 5.5796 and 'lift(ref)' $\approx$ 0.0106 for the 'flow around cylinder' benchmark problem at Re=20 (see [73] for the details).

In the following tests, we consider the case of convection dominated flow, for instance for medium and particularly high Re numbers, in combination with FEM methods. Then, numerical difficulties arise since the standard Galerkin formulation usually may lead to numerical oscillations and to convergence problems of the iterative solvers. Among the stabilization methods existing in the literature for these types of problems, especially for higher order finite elements, we use the *edge-oriented FEM stabilization* (EO-FEM) proposed in [71] which is based on the penalization of the gradient jumps over element boundaries [13]. In the 2D-case, the additional stabilization term $\mathbf{J}\boldsymbol{u}$, acting only on the velocity $\boldsymbol{u}$ in the momentum equations, takes the following form (with $h_E = |E|$)

$$\langle \mathbf{J}\boldsymbol{u}, \boldsymbol{v}\rangle = \sum_{\text{edge E}} \max(\gamma \frac{1}{\mathrm{R}e} h_E, \gamma^* h_E^2) \int_E [\nabla \boldsymbol{u}]_E : [\nabla \boldsymbol{v}]_E \, ds, \tag{46}$$

and can be simply added to the original bilinear form. Due to the linear character of this stabilization technique, efficient Newton-type and multigrid solvers can be quite easily applied to this kind of stabilization techniques (see [71] for more details, particularly regarding the parameters γ and γ^*). They have been applied also in the subsequent numerical tests.

As the test problem, we consider the well-known 'Standing Vortex' problem [33], in which case the incompressible Navier-Stokes equations for inviscid flow (R$e = \infty$)

$$\frac{\partial \boldsymbol{u}}{\partial t} + \boldsymbol{u} \cdot \nabla \boldsymbol{u} + \nabla p = 0, \quad \nabla \cdot \boldsymbol{u} = 0 \qquad \text{in } \Omega \times (0,T), \qquad \boldsymbol{u}(0) = \boldsymbol{u}_0\,, \tag{47}$$

are solved in the unit square $\Omega = (0,1)^2$. The initial value $\boldsymbol{u}_0$ is an axially symmetric vortex which also represents the exact steady-state solution. In polar coordinates, the velocity $\boldsymbol{u}$ can

be decomposed into the radial component $\boldsymbol{u}_r$ and the angular component $\boldsymbol{u}_\theta$. For the initial value $\boldsymbol{u}_0$ they are given by

$$\boldsymbol{u}_r = 0, \quad \boldsymbol{u}_\theta = \begin{cases} 5r, & r < 0.2, \\ 2 - 5r, & 0.2 \le r \le 0.4, \\ 0, & r > 0.4, \end{cases} \tag{48}$$

where $r = \sqrt{(x-0.5)^2 + (y-0.5)^2}$ denotes the distance from the center of Ω. We aim with the following simulations to check the robustness and accuracy of the edge-oriented stabilization in combination with the underlying finite element space in preserving the original vortex. Therefore, the numerical results produced by the different types of FEM spaces with edge-oriented stabilization techniques are compared with the exact solution in Fig. 8. They were obtained at $T = 3$ ('three rotations') on a successively refined mesh consisting of equidistant quadrilateral cells. It is obvious from these tests that the first order finite elements require at least two, resp., three more mesh refinements to produce similar results as obtained with the higher order nonconforming or conforming finite elements which capture the essential flow features at rather coarse level, without spurious numerical oscillations.

8 Conclusions

In this paper, we have discussed second order nonconforming finite elements as members of a new family of higher order approaches. As typical for nonconforming finite elements, numerical problems arise on perturbed grids which are still shape regular but which consist no longer of asymptotically affine equivalent mesh cells. As a remedy, we presented two new approaches via nonparametric basis functions ($\widetilde{Q}_2^n$-element) as well as via additional nonconforming cell bubble functions ($\widetilde{Q}_2^b$-element). For the last approach, we have proven optimal order of the approximation error and optimal estimates for the discretization error in the case of the Poisson problem. Moreover, we have discussed corresponding geometrical multigrid solvers which are based on the canonical full order grid transfer operators together with standard smoothing operators. Finally, we have shown prototypical numerical results for the incompressible Navier-Stokes equations, illustrating the high accuracy of the new $\widetilde{Q}_2^b$-element for a standard laminar flow configuration as well as for a convection dominated case in combination with special edge-oriented stabilization techniques. As a summary, the presented results illustrate that the proposed FEM-multigrid approaches appear to be very advantageous candidates for flow simulation tools which we currently extend to more complex flow situations in the 2D- as well as in the 3D-case.

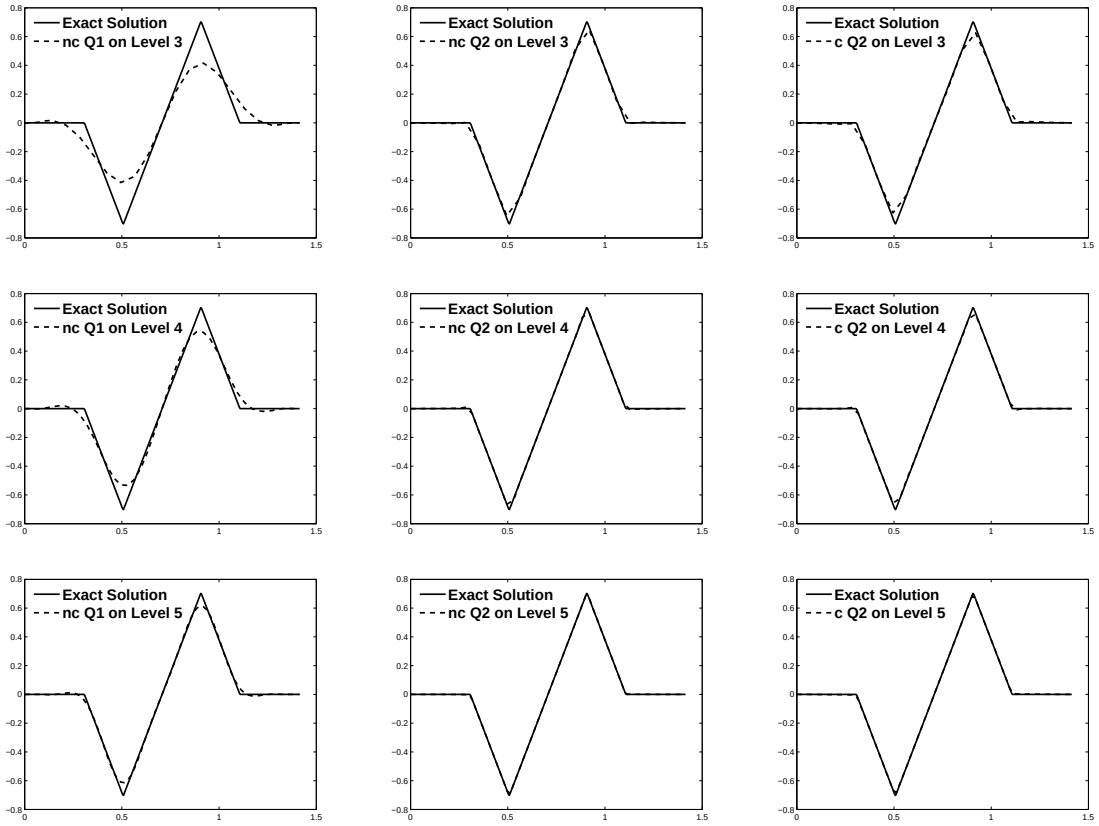

Figure 8: Cutline at y=0.5 of the y-velocity component for the 'Standing Vortex' example with EO-FEM stabilization for the different elements $\tilde{Q}_1/\mathbb{P}_0$ (LEFT), $\tilde{Q}_2/\mathbb{P}_1^{dc}$ (MIDDLE) and the conforming $Q_2/\mathbb{P}_1^{dc}$ (RIGHT) on three different mesh levels.

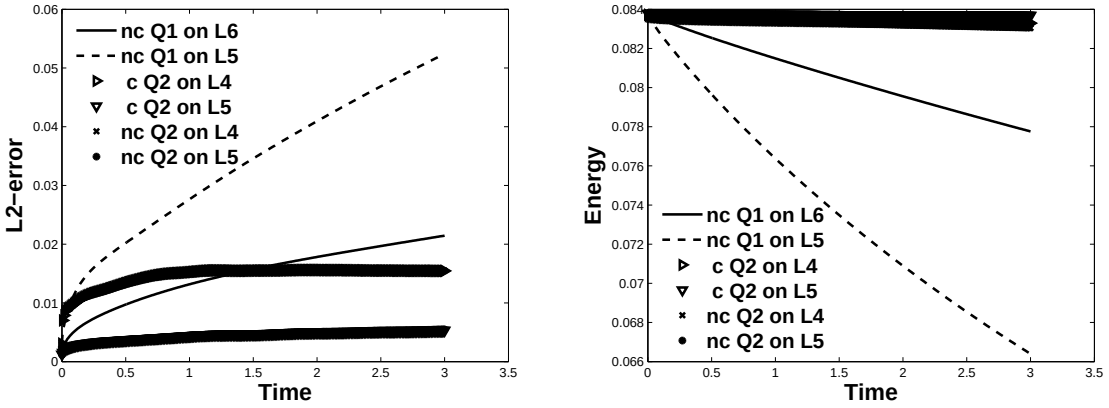

Figure 9: L_2-norm of the error and kinetic energy for the 'Standing Vortex' example with EO-FEM for $\tilde{Q}_1/\mathbb{P}_0$-, $\tilde{Q}_2/\mathbb{P}_1^{dc}$- and $Q_2/\mathbb{P}_1^{dc}$-elements on two different mesh levels.

References

[1] M. Ainsworth. Robust a posteriori error estimation for nonconforming finite element approximation. *SIAM J. Numer. Anal.*, 42(6):2320–2341, 2005.

[2] L. El Alaoui and A. Ern. Nonconforming finite element methods with subgrid viscosity applied to advection-diffusion-reaction equations. *Numer. Methods Partial Differential Equations*, 22(5):1106–1126, 2006.

[3] T. Apel and G. Matthies. Non-conforming, anisotropic, rectangular finite elements of arbitrary order for the Stokes problem. Bericht 374, Fakultät für Mathematik, Ruhr-Universität Bochum, 2006.

[4] T. Apel and G. Matthies. Nonconforming, anisotropic, rectangular finite elements of arbitrary order for the Stokes problem. *SIAM J. Numer. Anal.*, 46(4):1867–1891, 2008.

[5] D. Arnold, D. Boffi, and R.S. Falk. Approximation by quadrilateral finite elements. *Math. Comput.*, 71(239):909–922, 2002.

[6] D. Braess, M. Dryja, and W. Hackbusch. A multigrid method for nonconforming fe-discretisations with application to non-matching grids. *Computing*, 63(1):1–25, 1999.

[7] D. Braess and R. Verfürth. Multigrid methods for nonconforming finite element methods. *SIAM J. Numer. Anal.*, 27(4):979–986, 1990.

[8] S. C. Brenner. A nonconforming multigrid method for the stationary Stokes equations. *Math. Comp.*, 55:411–437, 1990.

[9] S. C. Brenner and L. R. Scott. *The mathematical theory of finite element methods.* Springer, 2002.

[10] F. Brezzi and M. Fortin. *Mixed and Hybrid Finite Element methods.* Springer, Berlin, 1986.

[11] S.H.M. Buijssen. *Numerische Analyse eines parallelen 3-D-Navier-Stokes-Lösers.* TU Dortmund, 2002. Diplomarbeit.

[12] S.H.M. Buijssen. parpp3d++ – a parallel HPC code for the incompressible nonstationary Navier—Stokes equations. In A. Bode, F. Durst, W. Hanke, and S. Wagner, editors, *High Performance Computing in Science and Engineering*, Transaction of the Second Joint HLRB and KONWIHR Result and Reviewing Workshop, pages 169–178. Springer, Berlin, March 2004. ISBN 3-540-44326-6.

[13] E. Burman. A unified analysis for conforming and nonconforming stabilized finite element methods using interior penalty. *SIAM J. Numer. Anal.*, 43(5):2012–2033, 2005.

[14] Z. Cai, Jr.J. Douglas, J.E. Santos, S. Dongwoo, and X. Ye. Nonconforming quadrilateral finite elements: a correction. *Calcolo*, 37(4):253–254, 2000.

[15] Z. Cai, Jr.J. Douglas, and X. Ye. A stable nonconforming quadrilateral finite element method for the stationary Stokes and Navier-Stokes equations. *Calcolo*, 36:215–232, 1999.

[16] C. Carstensen, S. Bartels, and S. Jansche. A posteriori error estimates for nonconforming finite element methods. *Numer. Math.*, 92(2):233–256, 2002.

[17] C. Carstensen and R. H. W. Hoppe. Convergence analysis of an adaptive nonconforming finite element method. *Numer. Math.*, 103(2):251–266, 2006.

[18] C. Carstensen and J. Hu. A unifying theory of a posteriori error control for nonconforming finite element methods. *Numer. Math.*, 107(3):473–502, 2007.

[19] C. Carstensen, J. Hu, and A. Orlando. Framework for the a posteriori error analysis of nonconforming finite elements. *SIAM J. Numer. Anal.*, 45(1):68–82, 2007.

[20] Z. Chen. On the convergence of Galerkin-multigrid methods for nonconforming finite elements. *East-West J. Numer. Math.*, 7(2):79–104, 1999.

[21] Z. Chen, D. Y. Kwak, and J. Y. Yoon. Multigrid algorithms for nonconforming and mixed methods for nonsymmetric and indefinite problems. *SIAM J. Sci. Comput.*, 19:502–515, 1998.

[22] Z. Chen and P. Oswald. Multigrid and multilevel methods for nonconforming Q1 elements. *Math. Comput.*, 67:667–693, 1998.

[23] P.G. Ciarlet. *The finite element method for elliptic problems.* Studies in mathematics and its applications, Vol. 4. North-Holland Publishing Company, Amsterdam, New-York, Oxford, 1978.

[24] M. Crouzeix and P.-A. Raviart. Conforming and nonconforming finite element methods for solving the stationary Stokes equations I. *RAIRO Anal. Numér.*, 7:33–76, 1973.

[25] H. Damanik, J. Hron, A. Ouazzi, and S. Turek. A monolithic FEM–multigrid solver for non–isothermal incompressible flow on general meshes. *Journal of Computational Physics*, 228:3869–3881, 2009.

[26] E. Dari, R. Durán, and C. Padra. Error estimators for nonconforming finite element approximations of the Stokes problem. *Math. Comp.*, 64(211):1017–1033, 1995.

[27] E. Dari, R. Duran, C. Padra, and V. Vampa. A posteriori error estimators for nonconforming finite element methods. *RAIRO Modél. Math. Anal. Numér.*, 30(4):385–400, 1996.

[28] Jr.J. Douglas, J.E. Santos, D. Sheen, and X. Ye. Nonconforming Galerkin methods based on quadrilateral elements for second order elliptic problems. *M2AN Math. Model. Numer. Anal.*, 33(4):747–770, 1999.

[29] M. Fortin and M. Soulie. A non-conforming piecewise quadratic finite element on the triangle. *Int. J. Numer. Meth. Engrg.*, 19(4):505–520, 1983.

[30] G.P. Galdi, R. Rannacher, A.M. Robertson, and S. Turek. *Hemodynamical Flows Modelling, Analysis and Simulation*, volume 37. Birkhäuser, 2008. OWS-Oberwolfach Seminars.

[31] I. Georgiev, J. Kraus, and S. Margenov. Multilevel preconditioning of rotated bilinear non-conforming fem problems. *Computers and Mathematics with Applications*, 55(10):2280–2284, 2008.

[32] M. Grajewski, J. Hron, and S. Turek. Dual weighted a posteriori error estimation for a new nonconforming linear finite element on quadrilaterals. *Applied Numerical Mathematics*, 54(3-4):504–518, 2005.

[33] P.M. Gresho and S.T. Chan. On the theory of semi-implicit projection methods for viscous incompressible flow and its implementation via a finite element method that also introduces a nearly consistent mass matrix. II: Implementation. *Int. J. Numer. Methods Fluids*, 11(5):621–659, 1990.

[34] Hou-De Han. Nonconforming elements in the mixed finite element method. *J. Comput. Math.*, 2:223–233, 1984.

[35] J.P. Hennart, J. Jaffré, and J.E. Roberts. A constructive method for deriving finite elements of nodal type. *Numer. Math.*, 53(6):701–738, 1988.

[36] R.H.W. Hoppe and B. Wohlmuth. Element-oriented and edge-oriented local error estimators for nonconforming finite element methods. *RAIRO Modél. Math. Anal. Numér.*, 30(2):237–263, 1996.

[37] J. Hron and S. Turek. *A monolithic FEM/Multigrid Solver for ALE formulation of fluid structure interaction with application in biomechanics*, volume 53 of *Lecture Notes in Computational Science and Engineering*. Bungartz, H.-J.; Schäfer, M., Springer, 2006. Fluid-Structure Interaction - Modelling, Simulation, Optimization,ISBN 3-540-34595-7.

[38] V. John, P. Knobloch, G. Matthies, and L. Tobiska. Non-nested multi-level solvers for finite element discretisations of mixed problems. *Computing*, 68(4):313–341, 2002.

[39] V. John, G. Matthies, F. Schieweck, and L. Tobiska. A streamline-diffusion method for nonconforming finite element approximations applied to convection-diffusion problems. *Comput. Methods Appl. Mech. Engrg.*, 166(1-2):85–97, 1998.

[40] V. John, J.M. Maubach, and L. Tobiska. Nonconforming streamline-diffusion-finite-element-methods for convection-diffusion problems. *Numer. Math.*, 78(2):165–188, 1997.

[41] V. John and L. Tobiska. A coupled multigrid method for nonconforming finite element discretizations of the 2D-Stokes equation. *Computing*, 64:307–321, 2000.

[42] G. Kanschat and F.-T. Suttmeier. A posteriori error estimates for nonconforming finite element schemes. *Calcolo*, 36(3):129–141, 1999.

[43] M. Köster and S. Turek. The influence of higher order FEM discretisations on multigrid convergence. *CMAM*, 6(2):221–232, 2006.

[44] D. Kuzmin and S. Turek. High-resolution FEM-TVD schemes based on a fully multidimensional flux limiter. *J. Comput. Phys.*, 198:131–158, 2004.

[45] D. Kuzmin and S. Turek. Multidimensional FEM–TVD paradigm for convection–dominated flows. In *Proceedings of the IV European Congress on Computational Methods in Applied Sciences and Engineering (ECCOMAS)*, volume II. nn, 2004. ISBN 951-39-1869-6.

[46] W.J. Layton, F. Schieweck, and I. Yotov. Coupling fluid flow with porous media flow. *SIAM J. Numer. Anal.*, 40(6):2195–2218, 2003.

[47] J. Lazaar and S. Nicaise. A nonconforming finite element method with anisotropic mesh grading for the incompressible Navier-Stokes equations in domains with edges. *Calcolo*, 39(3):123–168, 2002.

[48] H. Lee and D. Sheen. A new quadratic nonconforming finite element on rectangles. *Numer. Meth. PDEs*, 22(4):954–970, 2005.

[49] G. Lube and L. Tobiska. A nonconforming finite element methods of streamline diffusion type for the incompressible Navier-Stokes equations. *J. Comp. Math.*, 8(2):147–158, 1990.

[50] S. Mao, S. Chen, and D. Shi. Convergence and superconvergence of a nonconforming finite element on anisotropic meshes. *Int. J. Numer. Anal. Model.*, 4(1):16–38, 2007.

[51] G. Matthies. *Finite element methods for free boundary value problems with capillary surfaces*. PhD thesis, Fakultät für Mathematik, Otto-von-Guericke-Universität Magdeburg, 2002. published at Shaker-Verlag Aachen.

[52] G. Matthies. Inf-sup stable nonconforming finite elements of higher order on quadrilaterals and hexahedra. *M2AN Math. Model. Numer. Anal.*, 41(5):855–874, 2007.

[53] G. Matthies and F. Schieweck. On the reference mapping for quadrilateral and hexahedral finite elements on multilevel adaptive grids. *Computing*, 80(2):95–119, 2007.

[54] G. Matthies and F. Schieweck. Nonconforming finite elements of higher order satisfying a new compatibility condition. *J. Numer. Math.*, 16(1):23–50, 2008.

[55] G. Matthies and L. Tobiska. The inf-sup condition for the mapped Q_k/P_{k-1}^{disc} element in arbitrary space dimensions. *Computing*, 69(2):119–139, 2002.

[56] G. Matthies and L. Tobiska. Inf-sup stable non-conforming finite elements of arbitrary order on triangles. *Numer. Math.*, 102(2):293–309, 2005.

[57] H. Oswald. A parallel multigrid algorithm for solving the incompressible Navier–Stokes equations with nonconforming finite elements in three dimensions. *Proc. Parallel CFD'96*, 1996. Capri/Italy.

[58] H. Oswald. *Parallel Multigrid Algorithms for Solving the Incompressible Navier-Stokes Equations with Nonconforming Finite Elements in Three Dimensions*. PhD thesis, Universität Heidelberg, 1998.

[59] C. Park and D. Sheen. P_1-nonconforming quadrilateral finite element methods for second-order elliptic problems. *SIAM J. Numer. Anal.*, 41(2):624–640, 2003.

[60] R. Rannacher and S. Turek. Simple nonconforming quadrilateral Stokes element. *Numer. Methods Partial Differential Equations*, 8:97 – 111, 1992.

[61] F. Schieweck. A parallel multigrid algorithm for solving the Navier–Stokes equations. *IMPACT of Computing in Science and Engineering*, 5:345–378, 1993.

[62] F. Schieweck. *Parallele Lösung der stationären inkompressiblen Navier–Stokes Gleichungen*. Otto-von-Guericke-Universität Magdeburg, Fakultät für Mathematik, 1996. Habilitation.
`http://www-ian.math.uni-magdeburg.de/~schiewec/papers.html`.

[63] F. Schieweck. A posteriori error estimates with post-processing for nonconforming finite elements. *Math. Modelling and Numerical Analysis*, 36(3):489–503, 2002.

[64] F. Schieweck and L. Tobiska. A nonconforming finite element method of upstream type applied to the stationary Navier–Stokes equation. *Math. Modelling and Numerical Analysis*, 23(4):627–647, 1989.

[65] F. Schieweck and L. Tobiska. An optimal order error estimate for an upwind discretization of the Navier–Stokes equations. *Numerical Methods for Partial Differential Equations*, 12(407):421, 1996.

[66] P. Schreiber. *A New Finite Element Solver for the Nonstationary Incompressible Navier–Stokes Equations in Three Dimensions*. PhD thesis, Universität Heidelberg, 1996.

[67] D. Shi, S. Mao, and S. Chen. An anisotropic nonconforming finite element with some superconvergence results. *J. Comput. Math.*, 23(3):261–274, 2005.

[68] D. Shi and Y. Zhang. A nonconforming anisotropic finite element approximation with moving grids for Stokes problem. *J. Comput. Math.*, 24(5):561–578, 2006.

[69] M. Stynes and L. Tobiska. The streamline-diffusion method for nonconforming Q1rot-elements on rectangular tensor product meshes. *IMA Journal of Numerical Analysis*, 21:123–142, 2001.

[70] S. Turek. *Efficient solvers for incompressible flow problems*. Lecture Notes in Computational Science and Engineering. Springer, Berlin, 1999. volume 6.

[71] S. Turek and A. Ouazzi. Unified edge–oriented stabilization of nonconforming FEM for incompressible flow problems: Numerical investigations. *Journal of Numerical Mathematics*, 15(4):299–322, 2007.

[72] S. Turek, A. Ouazzi, and R. Schmachtel. Multigrid methods for stabilized nonconforming finite elements for incompressible flow involving the deformation tensor formulation. *Journal of Numerical Mathematics*, 10:235–248, 2002.

[73] S. Turek and M. Schäfer. Benchmark computations of laminar flow around cylinder. In R. Rannacher F. Durst, E. Krause, editor, *Flow Simulation with High-Performance*

Computers II, Notes on Numerical Fluid Mechanics (ed. Hirschel, E.H.), pages 547–566. Vieweg, 1996.